AR-006-950

ELECTRONICS RESEARCH LABORATORY

Electronic Warfare Division

RESEARCH REPORT
ERL-0617-RR

WIDEBAND GUIDED-WAVE PHOTONICS FOR ELECTRONIC WARFARE APPLICATIONS

Anthony C. Lindsay

ABSTRACT

The report reviews the basic state of the art of guided-wave photonics systems for microwave and millimetre wave Electronic Warfare (EW) applications. Examples of several architectures are presented, and the results discussed in terms of Australian technological capability and current research in Electronic Warfare Division.

MARCH 1992

APPROVED FOR PUBLIC RELEASE

Postal Address: Director, Electronics Research Laboratory,
PO Box 1500, Salisbury, South Australia, 5108.

ERL-0617-RR

CONTENTS

1 INTRODUCTION 1
2 BASIC FIBRE-OPTIC LINK CALCULATIONS 2
2.1 Introduction 2
2.2 Directly-Modulated RF Fibre-Optic Links 2
2.2.1 Direct Modulation of Laser Diodes 2
2.2.2 The Link Model 3
2.2.3 Link Insertion Loss 3
2.2.4 Noise in a Directly Modulated Link 6
2.2.4.1 Relative Intensity Noise (RIN) 6
2.2.4.2 Thermal Noise at the Receiver 7
2.2.4.3 Shot Noise 7
2.2.4.4 Comparison of Noise Contributions 8
2.2.5 Laser Diode Non-Linearity 9
2.3 Externally-Modulated RF Fibre-Optic Links 11
2.3.1 External Modulators 11
2.3.2 The Link Model 12
2.3.3 Link Insertion Loss 13
2.3.4 Noise in an Externally Modulated Link 16
2.3.5 Modulator Non-Linearity 17
2.4 A Comparison of Link Architectures 23
2.4.1 Introduction 23
2.4.2 Bandwidth 24
2.4.3 Sensitivity 24
2.4.4 Dynamic Range 25
2.4.5 Conclusions 25
3 SOME FIBRE-OPTIC LINK APPLICATIONS 26
3.1 Introduction 26
3.2 The "Remote Transmitter" Scenario 26
3.3 The "Remote Receiver" Scenario 29
3.4 Near-Future Improvements in Link Performance 30
3.5 Reduction of Transducer Non-linearities and Noise 32
4 DELAY LINE SIGNAL PROCESSING - THE OPTICAL IFM 38
4.1 Introduction 38
4.2 Theory of Operation 38
4.3 Some Preliminary Numbers 40
4.4 Testing the Frequency Response of a Fibre-Optic Microwave Interferometer 41
4.5 Optical IFM - General System Considerations 47

4.6 The Role of Bulk Optics 54
5 CONCLUSIONS 56
5.1 Introduction 56
5.2 Wideband Photonics Research in Electronic Warfare Division 56
5.3 Possible Research Projects 58
5.4 Addendum 59
REFERENCES 61

LIST OF TABLES

1 Countries with Significant National R&D Efforts 57

LIST OF FIGURES

2.1 Model for directly modulated fibre optic link 3
2.2 Response of a typical high frequency laser diode (from Ref 1) 11
2.3 Typical laser diode parameters 11
2.4 Basic external modulator architectures 12
2.5 Model for externally modulated fibre optic link 13
2.6 Modulator optical output power vs relative input voltage 14
2.7 Small signal link parameters for system E2 17
2.8 Dynamic range calculation for system E1 21
2.9 Dynamic range calculation for system E2 21
2.10 Dependence of dominant non-linearity on phase error 22
2.11 Dynamic range calculation for E2 with 10° phase error 23
3.1 Fibre optic architecture for submarine EW mast 27
3.2 Fibre optic architecture for aircraft towed decoy 29
3.3 Linearisation of integrated optical modulator response 32
3.4 Linearisation modelling results 35
3.5 Linearisation modelling results 35
3.6 Improvement in single tone dynamic range due to feed forward linearisation 36
3.7 Linearisation of laser diode response and reduction of RIN 36
3.8 Electro-optic "noise-eater" using feed-forward architecture 37
4.1 Fibre optic interferometer 38
4.2 Cascaded fibre interferometer for microwave frequency measurement 42
4.3 Output from signal generator 43
4.4 Normalised system frequency response from output #1 44
4.5 Fibre interferometer response 44
4.6 Fibre interferometer response 45
4.7 Response from output #3 46
4.8 Optical IFM architecture 47
4.9 Uncertainty in frequency determination due to noise 48

4.10 Frequency resolution of fibre IFM as a function of SNR..... 52
4.11 Schematic showing how a single set of interferometers can be used for different frequency regions..... 54
4.12 A tunable bulk optic interferometer..... 55
4.13 Cascaded microwave Mach-Zehnder interferometers..... 55

THIS IS A BLANK PAGE

1 INTRODUCTION

In the last four years substantial improvements in the bandwidth, insertion loss and production quality of high speed semiconductor lasers and integrated optical modulators, and the advent of all-optical amplification techniques, has led to the rapid emergence of these devices as viable contenders for use in microwave and millimetre wave Electronic Warfare (EW) applications.

In the case of integrated optics, no other single technology has the demonstrated bandwidth capability to cover the range from HF up to millimetre wave frequencies using basically the same device designs, fabrication materials and manufacturing techniques. The extremely low losses of optical fibre and optical fibre components allows very large, dispersionless (as far as the microwave signal is concerned) transmission distances to be achieved before signal re-amplification is required. All-optical amplification techniques hold the promise of extremely wide bandwidth microwave signal amplification, and therefore totally lossless transmission over unprecedented distances. The spatial compression of the microwave information means that optical microwave components such as couplers, switches etc can be placed within tens of microns of each other and still have essentially perfect isolation, thereby allowing smaller networking and faster routing of signals. It is only in the last few years however that the technology has matured to the stage where useful (though often far from ideal) systems can be constructed from commercially available components.

This report concentrates almost exclusively on guided-wave technologies ie integrated optics and fibre optics. This is mainly due to the belief held by the author that these technologies are most likely to overcome the traditional difficulties associated with making optical EW systems robust enough for the tactical environment - a common and often justified criticism of optical techniques in general.

It is the purpose of this research report to examine the application of high-speed optical modulation technologies to future EW systems. This report is by no means totally inclusive. Some potentially high payoff areas such as optical techniques for millimetre wave generation and distribution, and optical electromagnetic impulse generation are not addressed, and considerations such as tailoring modulator response for enhanced efficiency at specific centre frequencies and bandwidths are not discussed. The view has been to pursue performance covering very wide bandwidths - either the full 18 GHz currently of interest or the full 40 GHz required by emerging electromagnetic environments. The systems are assumed to rely on direct detection rather than coherent detection of the modulating signal, due to the superior robustness and relative simplicity of direct detection systems.

The two basic wideband modulation techniques, direct and external modulation, are introduced in Section 2. The fundamental equations describing insertion loss, noise contributions and sources of non-linearities are derived in Sections 2.2 and 2.3. A comparison of link architectures based upon the generic requirements of the EW scenario and the capabilities of Australian industry and research institutions is undertaken in Section 2.4. It is hoped that these considerations will form some basis for decisions taken concerning the direction of electro-optic research in Electronic Warfare Division.

Section 3 introduces two generic EW scenarios, and describes fibre-optic link applications appropriate to each scenario by exploiting currently available off-the-shelf technology. Section 3.4 gives an example of the capabilities of next generation technology by examining a wide-band link which is composed of state-of-the-art components that have been demonstrated in various laboratories. Finally Section 3.5 addresses the outstanding problem of reduction of device non-linearities, in order to improve both sensitivity and dynamic range performance.

In Section 4 a proposal and some very preliminary results for an all-optical fibre correlator for use in either instantaneous frequency measurement or angle of arrival determination are outlined.

The report conclusions and proposals for future research directions are summarised in Section 5.

2 BASIC FIBRE-OPTIC LINK CALCULATIONS

2.1 Introduction

In this section the basic equations used to perform calculations of insertion loss, noise contributions, dynamic range etc for both directly and externally modulated fibre-optic RF links are presented. Section 2.2 deals with the various aspects of directly modulated links, and Section 2.3 deals with externally modulated links. A comparison of the link architectures and the impact of limiting factors such as laser relative intensity noise and device non-linearity are given in Section 2.4. The conclusions are presented in terms of appropriate resource allocation based on the current capabilities of Australian technology and system requirements unique to Electronic Warfare. Actual system examples are deferred until Section 3.

2.2 Directly-Modulated RF Fibre-Optic Links

2.2.1 Direct Modulation of Laser Diodes

In the case of direct modulation, the RF signal is superimposed onto the laser bias current, thereby yielding an intensity modulation of the optical beam. Depending upon the details of laser construction (Ref 1), bandwidths of up to 30 GHz (Ref 2) have been achieved in the laboratory. The limiting frequency of modulation is characterised by the occurrence of a resonance oscillation peak in the frequency response of the diode. The diode frequency response tends to be quite flat up to the resonance peak, after which the response falls off at roughly 40 dB/decade. The dynamics of the laser's active medium which give rise to this behaviour can be modelled by the rate equations (Ref 3)

$$\frac{dN}{dt} = \frac{I}{Ve} - \frac{N}{\tau} - A(N - N_{th})P \qquad (2.1a)$$

$$\frac{dP}{dt} = A(N - N_{th})P\gamma - \frac{P}{\tau_P} \qquad (2.1b)$$

where

N - injected electron (and hole) density

P - photon density in the active region

I - total current

V - volume of the active region

e - electronic charge (1.602×10^{-19} C)

τ - spontaneous recombination lifetime

τ_p - photon lifetime (through losses)

γ - confinement factor

N_{th} - threshold inversion population density

A - optical gain coefficient

From the steady-state solutions of Equations (2.1), the resonance frequency is readily derived as

$$\omega_r = \sqrt{\frac{AP_o}{\tau_p} - \frac{1}{2}\left(\frac{1}{\tau} + AP_o\right)^2} \qquad (2.2)$$

where P_o is the photon density in the steady state.

Equation (2.2) indicates that for high-speed response, the photon lifetime should be decreased, the optical gain increased and the confinement and photon density should be as high as possible. The degree to which these conditions can be achieved is limited by optical damage to the facets of the laser diode and thermal damage due to high injection currents.

Theoretical analysis of strained-quantum well lasers indicates theoretical limits of the order of 90 GHz bandwidth (Ref 4). Commercially available packaged laser diode modules currently have maximum operating bandwidths of about 10 - 12 GHz (Ref 5,6). Major limiting factors in extending the frequency range appear to be both acceptable laser performance and packaging. For example, Lasertron have had a USAF contract to develop 20 GHz bandwidth laser diodes since 1988. To the knowledge of the author, this contract has not yet resulted in a deliverable item.

2.2.2 The Link Model

Figure 2.1 shows the simple model used for the direct-modulated link calculation (Ref 7). The laser transmitter and receiver are treated as "off-the-shelf" packaged modules, consistent with the current use of the devices in Electronic Warfare Division. The input impedance R_{in} of the laser module includes both the intrinsic diode impedance (typically of the order of 5 Ω) and any input matching impedance (so that R_{in} = 50 Ω is usual). The photodiode module is modelled as a current source (the photodiode) and an impedance R_o consisting of a parallel combination of the actual photodiode impedance (typically 1 - 2 kΩ) and a matching impedance (again 50 Ω is usual). Reactive components such as those representing the photodiode junction capacitance etc are ignored in this simple model, however they are readily incorporated (Ref 1,8) for a more complete analysis by programs such as EEsof if required.

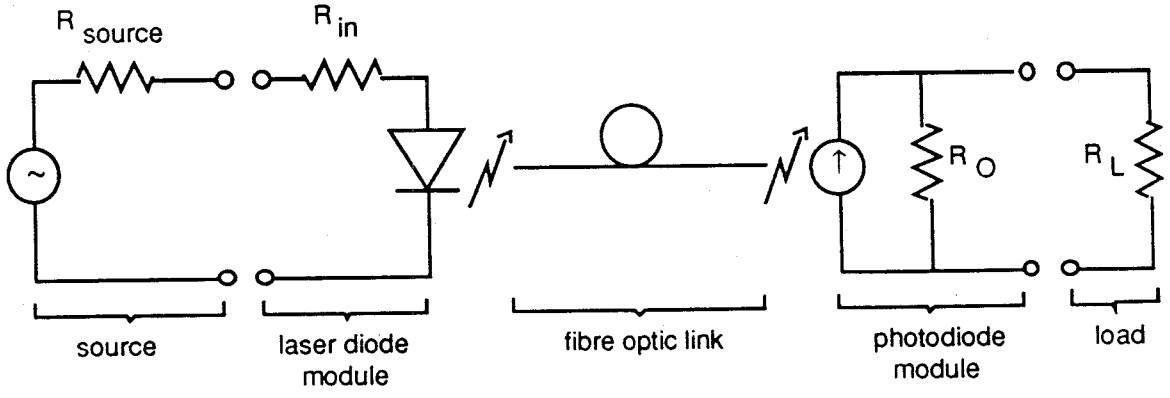

Figure 2.1 Model for directly modulated fibre optic link.

2.2.3 Link Insertion Loss

While there are quite a number of fundamental factors that affect the insertion loss of a fibre optic link - such as the gain medium confinement factor and laser external differential efficiency - when buying a packaged laser transmitter these considerations are combined into a single figure of merit known as the modulation gain. The modulation gain is essentially electrical to optical conversion efficiency, and as such has the units mW/mA.

For a given modulation gain M and input current i_{in}, the useful optical power coupled into the fibre is just

$$P_o = Mi_{in} \tag{2.3}$$

The useful power incident onto the photodiode is

$$P_{pd} = Mi_{in}\,\alpha_T \tag{2.4}$$

where α_T is the total optical loss of the link, including fibre splice losses, fibre attenuation and fibre-detector coupling loss.

The photodiode will convert the photon flux into an electrical signal with a quantum efficiency η (ie the number of electron-hole pairs generated per incident photon of energy $h\nu$), leading to a photodiode responsivity (for a PIN photodiode) of

$$r = \frac{\eta e}{h\nu} \quad \text{mA/mW} \tag{2.5}$$

resulting in a photodiode current of

$$i_{pd} = r\,P_{pd} \tag{2.6a}$$

$$= r\,Mi_{in}\,\alpha_T \tag{2.6b}$$

From Figure 2.1, the voltage drop V_{out} across the parallel load is just

$$V_{out} = i_{pd}\left(\frac{R_o\,R_L}{R_o + R_L}\right)$$

giving

$$i_{out} = i_{pd}\left(\frac{R_o}{R_o + R_L}\right)$$
$$= \left(\frac{R_o}{R_o + R_L}\right) r\,Mi_{in}\,\alpha_T \tag{2.7}$$

The link gain, accounting for matching losses into the transmitter module and out of the receiver module (given by $\sigma = 1-|\Gamma|^2$, where Γ is the usual voltage reflection coefficient), can now be written

$$\rho_G = \frac{i_{out}^2\,R_L\,\sigma_{RX}}{i_{in}^2\,R_{in}\,\sigma_{TX}}$$

ie

$$\rho_G = \left[\left(\frac{R_o}{R_o + R_L}\right) r\,M\,\alpha_T\right]^2 \frac{\sigma_{RX}}{\sigma_{TX}}\,\frac{R_L}{R_{in}} \tag{2.8a}$$

Equation 2.8a clearly shows the importance of reducing any optical loss terms, since they contribute as the square to the insertion loss. For the purposes of this report, it is convenient to define the link insertion loss as

$$\rho_L(\text{dB}) = -\,10 \log \rho_G \tag{2.8b}$$

It is also occasionally convenient to separate the terms of Equation 2.8a as

$$\rho_L(dB) = -\ 10 \log \left[\left\{ \left(\frac{R_o}{R_o + R_L} \right) r\, M \right\}^2 \frac{\sigma_{RX}}{\sigma_{TX}} \frac{R_L}{R_{in}} \right] - 20 \log \alpha_T$$

ie

$$\rho_L(dB) = L.L.\ (dB) + 2 \times O.L.\ (dB) \qquad (2.9)$$

where L.L. (dB) is the electrical insertion loss of the receiver and transmitter modules and O.L. (dB) is the optical loss of the link. This distinction is often useful since the total L.L. (dB) is often specified when buying an "off-the-shelf" fibre optic link. It is appropriate however, for the purposes of this section, to use Equation 2.8a.

Typical values for detector responsivity, modulation gain and module return losses are (Ref 5,6)

$r = 0.6 - 0.8$ mA/mW

$M = 0.02 - 0.04$ mW/mA

$\sigma_{TX}, \sigma_{RX} > 10$ dB

Some typical values for link optical losses are (Ref 9,10,11)

$\alpha_{opt} = 0.2 - 0.4$ dB/km (fibre attenuation loss)

$\alpha_f = 0.03 - 0.05$ dB/splice (multimode/single mode fusion splice loss)

$\alpha_c = 0.1 - 0.3$ dB (typical coupler insertion loss)

So, using the specifications for a typical 10 GHz bandwidth link (the Ortel 3510B/4510B (Ref 7))

$r = 0.7$ mA/mW

$M = 0.03$ mW/mA

$R_{in} = R_o = R_L = 50\ \Omega$

$\sigma_{TX} = \sigma_{RX} = 0.95$ (assumed values)

then Equation 2.8b gives an expected electrical insertion loss (ignoring optical losses) of

$$\rho_L = 40.0 \text{ dB} \qquad (2.10)$$

Both the Lasertron Q-LINK-10 (Ref 5) and Ortel (Ref 6,7) systems specify insertion losses of < 35 dB.

It is interesting to note the substantial improvement in link insertion loss if the trouble is taken to reactively match both the input to the ~ 5 Ω of the laser diode and the output to the ~ 1 kΩ of the photodiode (this is of course extremely difficult to achieve over the full operating bandwidths of interest, however it is beneficial to do the calculation to get some idea of "best possible" device performance for which to aim). Then the specifications become

$r = 0.7$ mA/mW

$M = 0.03$ mW/mA

$R_{in} = 5\ \Omega$

$R_o = R_L = 1\ k\Omega$

$\sigma_{TX} = \sigma_{RX} = 1$

and from Equation 2.8b

$$\rho_L = 16.6\ dB \tag{2.11}$$

Improving the performance of the devices further would require an improvement in the actual material and device design/construction parameters that determine the modulation gain M and the photodiode responsivity r. Actual component fabrication and design issues for high speed optoelectronic components are, at the moment, of limited interest to Electronic Warfare Division (although it is recognised that in the future, as local expertise grows, these factors may become subjects of active research). As shall be shown in the next section and discussed further in Section 2.4, for EW applications the potential gains of improved insertion loss are somewhat offset by link noise contributions in directly modulated links.

2.2.4 Noise in a Directly Modulated Link

In this section the contribution of various noise sources associated with a directly modulated link will be addressed. The three primary sources, the relative intensity noise of the diode laser, the thermal noise of the receiver and the shot noise of the photon field will be treated in detail. Minor noise sources such as post-amplifier noise, reflection noise etc will be briefly considered at the end of the section.

2.2.4.1 Relative Intensity Noise (RIN)

The relative intensity noise (RIN) is the ratio of the mean square power fluctuations to the square of the mean power, ie (Ref 7,12)

$$RIN \equiv \frac{\langle \Delta P^2(f) \rangle}{P_o^2} \tag{2.12}$$

These fluctuations are due to the shot noise processes associated with carrier injection and recombination within the active layer and have an intensity spectrum which is characterised by a broad and pronounced resonance at ω_r (Ref 12). If the modulation gain M was independent of frequency (which it is not, but it is an appropriate first approximation), then

$$RIN \approx \frac{\langle \Delta I^2 \rangle}{(I - I_{TH})^2} \tag{2.13}$$

when $\langle \Delta I^2 \rangle$ is the mean square of the current fluctuations that would produce the observed intensity fluctuations if the laser were noiseless, and $(I-I_{TH})$ is the operating current above the threshold I_{TH}. Since the input impedance is R_{in}, an equivalent noise power EIN_L can be defined via (Ref 7)

$$EIN_L \equiv \langle \Delta I^2 \rangle R_{in} = RIN\,(I-I_{TH})^2\,R_{in} \qquad (2.14)$$

Thus, the equivalent input noise EIN_L is the noise at the RF input of the laser that would produce the observed noise power if the laser itself were noiseless. Some typical values are (Ref 7)

$I-I_{TH}$ = 40 mA

R_{in} = 50 Ω

RIN = -140 dB/Hz

giving

$$EIN_L = -121 \text{ dBm/Hz} \qquad (2.15)$$

It is interesting to note the potential improvement in this figure that can be obtained by reactively matching the input to 5 Ω, as was done to reduce the insertion loss (Equation 2.11). From Equation 2.14 it is clear that the EIN will improve by 10 dB to EIN_L = -131 dBm/Hz. The significance of this is investigated in Section 2.2.4.4.

2.2.4.2 Thermal Noise at the Receiver

Thermal noise is due to the natural chaotic motion of free charge carriers that have an average kinetic energy kT. The thermal noise current variance is given by the well-known expression by Nyquist (Ref 13)

$$\langle i_{TH}^2 \rangle = \frac{4kTB}{R_L} \qquad (2.16)$$

where B is the detection bandwidth. Expressing Equation 2.16 as the available output power density referred back to the input of the laser diode gives

$$EIN_{TH} = \frac{kT}{\rho_G} \qquad (2.17)$$

where ρ_G is the link gain, Equation 2.8a.

2.2.4.3 Shot Noise

Shot noise arises due to the quantum nature of the photon field which results in fluctuations in the number of charge carriers attempting to diffuse across the potential barrier of the semiconductor junction of the photodiode. The shot noise is given by (Ref 13)

$$\begin{aligned} \langle i_s^2 \rangle &= 2e\bar{i}_{pd}B \\ &= 2er\bar{P}_{pd}B \end{aligned} \qquad (2.18)$$

The shot noise power delivered to the parallel load is

$$\begin{aligned} P_s &= \langle i_{out}^2 \rangle R_L \\ &= \langle i_s^2 \rangle \left(\frac{R_o}{R_o + R_L} \right)^2 R_L \end{aligned}$$

The noise power is taken to be that noise which occurs when $R_o = R_L$, and so

$$P_s = \frac{1}{2} e\, r\, R_L\, \bar{P}_{pd}\, B$$

which, as a power density referred back to the input is

$$EIN_s = \frac{1}{2\rho_G} e\, r\, R_L\, \bar{P}_{pd} \qquad (2.19)$$

2.2.4.4 Comparison of Noise Contributions

In order to clarify the relative magnitudes of each of the noise sources, it is appropriate to recall Equations 2.15, 2.17 and 2.19, ie

$$EIN_L = -\ 121\ \text{dBm/Hz} \qquad (2.20a)$$

$$EIN_{TH} = \frac{kT}{\rho_G}\ \text{W/Hz} \qquad (2.20b)$$

$$EIN_s = \frac{1}{2\rho_G} er\, R_L\, \bar{P}_{pd}\ \text{W/Hz} \qquad (2.20c)$$

Also, recalling the typical values of the various parameters

k = 1.38×10^{-23} W/Hz

T = 295 K

ρ_G = -35 dB = 3.162×10^{-4} (neglecting optical losses)

e = 1.602×10^{-19} C

r = 0.7 mA/mW

R_L = 50 Ω

$\bar{P}_{pd}$ = $M\,(I-I_{TH})$ = 1.2 mW

gives

$$EIN_L = -\ 121\ \text{dBm/Hz} \qquad (2.21a)$$

$$EIN_{TH} = -\ 139\ \text{dBm/Hz} \qquad (2.21b)$$

$$EIN_s = -\ 140\ \text{dBm/Hz} \qquad (2.21c)$$

It will be useful to denote by "D1" a directly modulated fibre-optic link with the above parameters, which essentially define a typical 10 GHz bandwidth off-the-shelf system (Ref 5,6).

It is apparent from Equations 2.21 that the limiting noise source is the noise of the laser diode itself. Only for very long links do thermal noise and shot noise play a significant role. For example, assuming an optical attenuation loss of 0.3 dB km^{-1}, the fibre link would have to be 30 km in length (ρ_L = 53 dB) before the thermal equivalent input noise was comparable to the laser equivalent input noise.

The potential improvements in system performance offered by impedance matching have been referred to briefly in previous sections. For comparison purposes it is useful to define a system "D2" in which the input to the laser diode is perfectly reactively matched to 5 Ω and the output perfectly matched to the photodiode impedance of 1 kΩ. As derived in Equation 2.11 such a link has an insertion loss of ~17 dB and the equivalent input noise contributions

$$EIN_L = -131 \text{ dBm/Hz}$$

$$EIN_{TH} = -157 \text{ dBm/Hz}$$

$$EIN_S = -145 \text{ dBm/Hz}$$

These results indicate that irrespective of whether impedance matching of the input and output is undertaken, the fundamental limitation on link performance is always the intrinsic noise of the transduction stage. In fact, the improvement in link performance can be clearly divided into two sections. Matching of the input improves both the sensitivity and insertion loss, whereas impedance matching of the photodiode improves link insertion loss - it has *no* effect on the ultimate link sensitivity. Since sensitivity is a fundamentally more important parameter in EW systems than insertion loss, this suggests that impedance matching of laser diodes is (initially at least) a more beneficial research direction than impedance matching of photodiodes.

Other minor noise sources include pre- and post-amplification noise, mode-partition noise (if multi-mode fibre is used) and reflection induced noise. Most amplifiers have noise figures of < 5 dB, which, for directly modulated links, would contribute a noise component negligible compared to EIN_L. Mode-partition noise is easily avoided by using single-mode fibre, as is usually the case with large bandwidth systems. Reflection-induced noise causes periodic spikes in the noise floor and can substantially increase the laser RIN by coupling back into the lasing modes, thereby causing their phases to vary (Ref 13). This means that optical isolators must be a feature of all microwave fibre-optic links, to prevent degradation of the laser RIN due to spurious reflections.

2.2.5 Laser Diode Non-Linearity

A laser diode is not a perfectly linear device, ie the output intensity does not vary linearly with input current for all possible values of the input current. As a consequence higher-order harmonics and intermodulation products are produced. Unlike communications systems where only third-order intermodulation products (IMP's) are of concern (since they may lie in the communication band being used), the EW scenario requires that all harmonic products be insignificant, since these may be misinterpreted as threat signals.

It has been demonstrated experimentally (Ref 1) that regardless of the constructional features of the laser diode, the levels of distortion are the same for all laser diodes with a given ω_r and optical modulation depth (OMD). The significant features are (Ref 1)

(1) The relative amplitudes of the second and third harmonic have maxima at frequencies near $\omega_r/2$. Typical values are -8 dBc and -18 dBc for second and third harmonics respectively at $\omega_r/2$ with an OMD of 0.8.

(2) The relative magnitude of the second harmonic increases as the square of the OMD at a fixed ω_r.

(3) The relative amplitude of the IMP has maxima at frequencies near $\omega_r/2$ and ω_r, with the level at ω_r being higher. Typically, for an OMD of 0.8, the magnitude of the IMP is -25 dBc and -30 dBc at ω_r and $\omega_r/2$ respectively.

(4) The relative amplitude of the IMP increases as the cube of the OMD at a fixed ω_r.

(5) The relative amplitude of both the second harmonic and the IMP decreases rapidly below $\omega_r/2$.

(6) Lasers with large resonance peaks in the small signal frequency response also exhibit pronounced maxima in the distortion curves.

Figure 2.2 shows schematically the behaviour of the various distortion products (Ref 1).

The magnitude of the distortion products clearly determines the maximum input power and therefore the link dynamic range. Since the third-order intermods behave as expected (point 4 above), the usual small-signal definition of the spurious free dynamic range (SFDR) can be used to define the link dynamic range ie

$$SFDR = \frac{2}{3}(TOI - P_{min}) \qquad (2.22)$$

where TOI is the third-order intercept and P_{min} is the minimum detectable signal (related to the EIN of the link). An alternative, large-signal definition of the dynamic range is

$$D.R. = P_{1dB} - 10 - P_{min} \qquad (2.23)$$

ie the dynamic range is the difference between the minimum detectable signal and that power that is 10 dB below the 1 dB compression point. In this report Equation 2.22 is generally used to define dynamic range.

Typical values for the TOI and P_{1dB} are (Ref 7)

TOI = + 27 dBm

P_{1dB} = + 13 dBm

Figure 2.3 shows a typical laser diode response curve, showing TOI, noise floor etc.

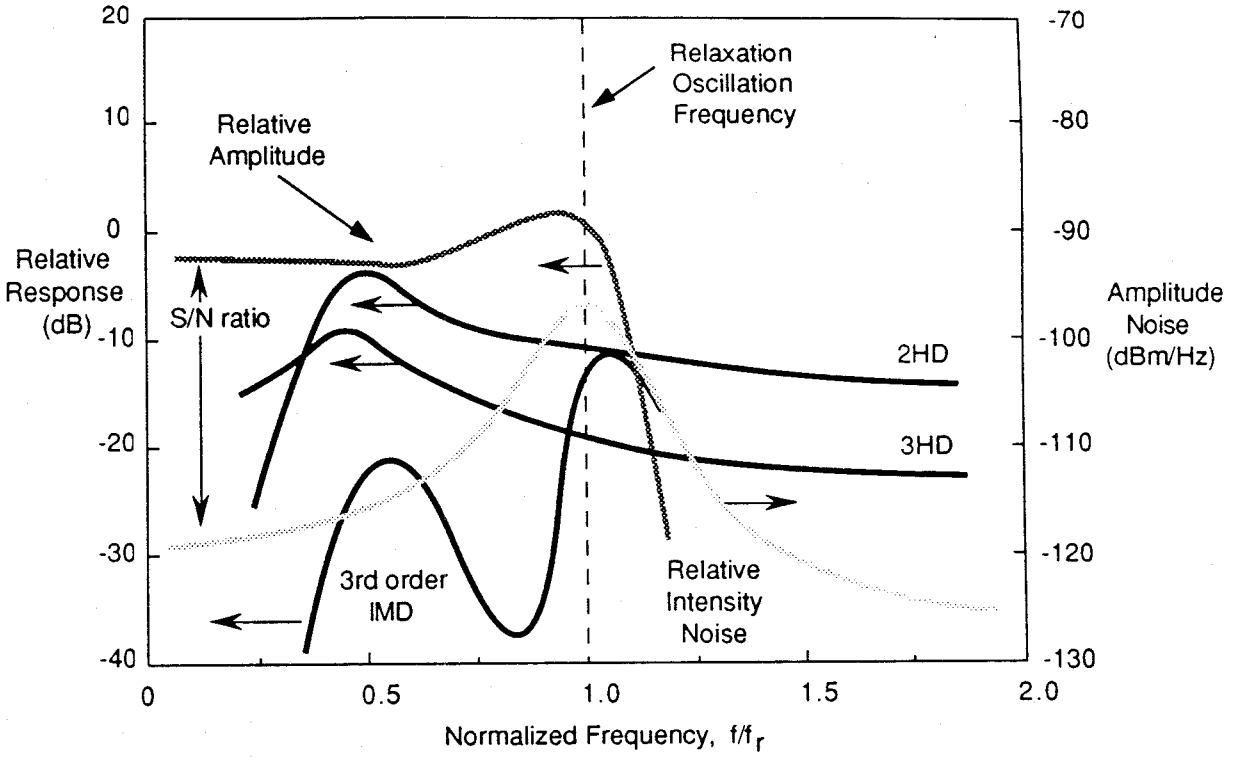

Figure 2.2 Response of a typical high frequency laser diode (from Ref 1).

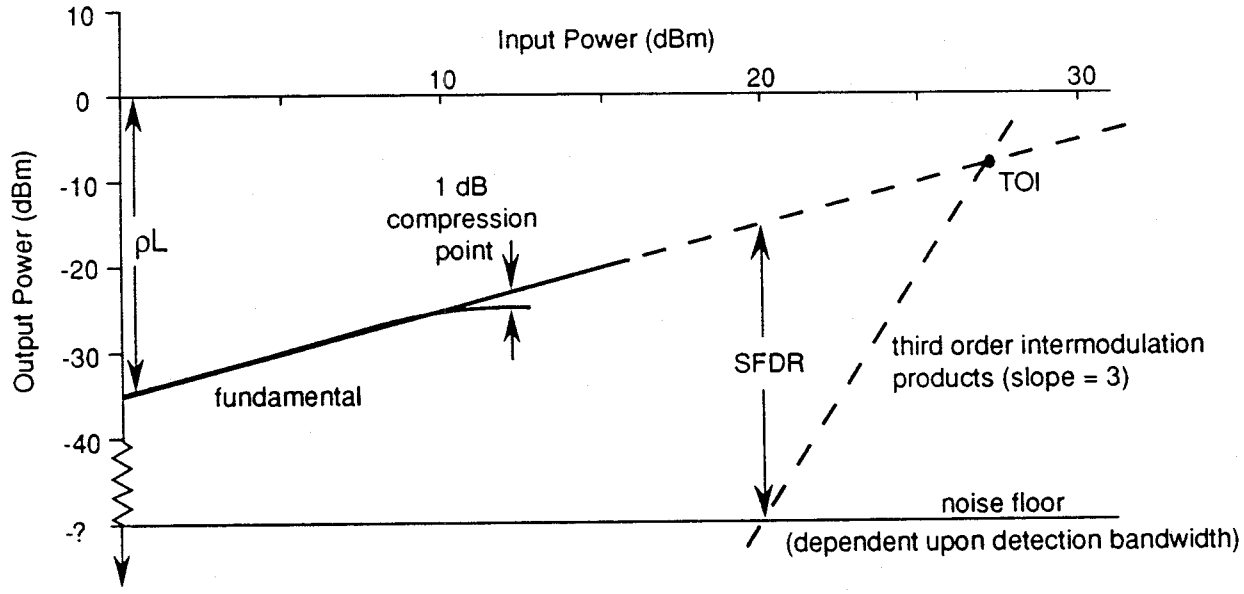

Figure 2.3 Typical laser diode parameters.

2.3 Externally-Modulated RF Fibre-Optic Links

2.3.1 External Modulators

In the case of external modulation, a cw laser source is modulated by exploiting the electro-optic effect, ie the change in refractive index that occurs in some crystals when subject to an electric field. The changing refractive index, caused by the microwave signal, is used to

phase modulate the cw laser beam. This phase modulation is converted to an intensity modulation by using either a Mach-Zehnder configuration (Ref 14) or by changing the coupling between two parallel integrated optical waveguides (Ref 15) - the "directional-coupler" configuration. Figure 2.4 shows the basic layout for these devices.

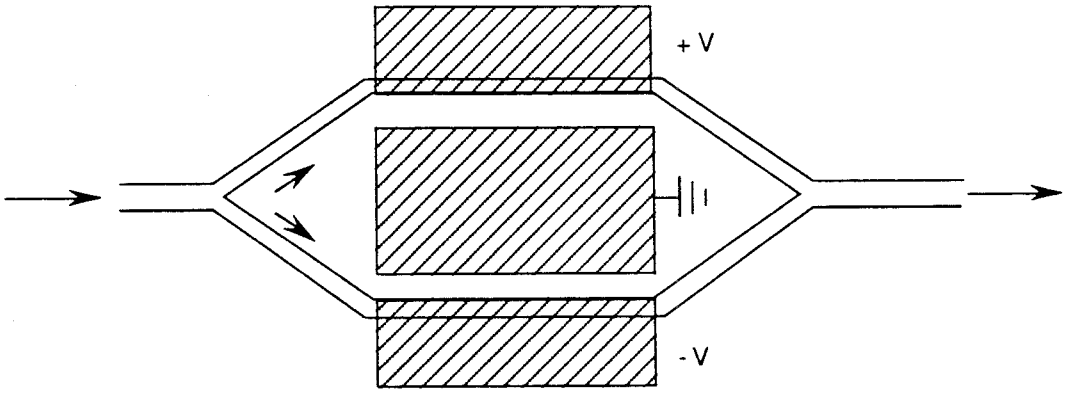

(a) Mach-Zehnder

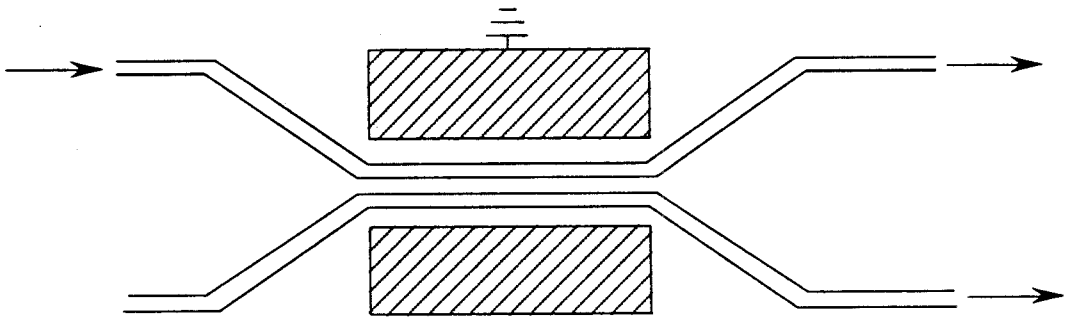

(b) Directional Coupler

Figure 2.4 Basic external modulator architectures.

External modulators have demonstrated much greater bandwidths than directly modulated laser diodes, the current records being 40 GHz in $LiNbO_3$-based devices (Ref 15,16) and 110 GHz in a GaAs device (Ref 17). Commercial devices with bandwidths up to 18 GHz (Ref 18) are available.

2.3.2 The Link Model

Figure 2.5 shows the simple link model used in this section. The photodiode module is treated as an "off-the-shelf" package as in Section 2.2.

The electrodes of a travelling wave electro-optic modulator are basically microstrip transmission line structures, and so the RF matching loss can be characterised by the usual transmission line voltage reflection coefficient $|\Gamma|$ or, in the case of an "off-the-shelf" module, the usual return loss σ_{TX}. The modulator is assumed to be of the Mach-Zehnder interferometric type.

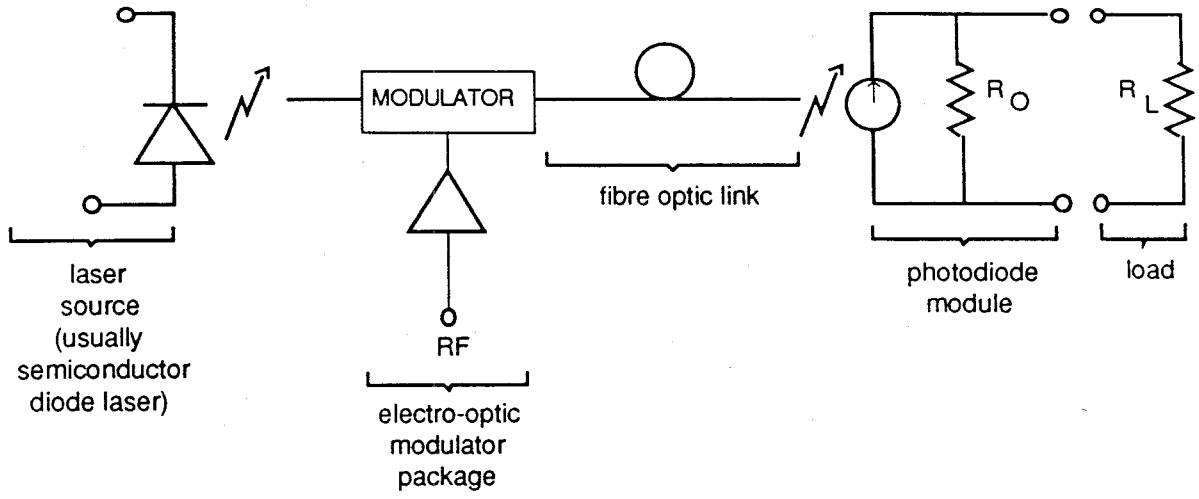

Figure 2.5 Model for externally modulated fibre optic link.

2.3.3 Link Insertion Loss

The voltage-optical intensity relationship for an interferometric modulator is (Ref 19)

$$P_m = \alpha_m P_o \cos^2\left[\frac{\pi V_{in}}{2 V_\pi} + \frac{\phi}{2}\right] \tag{2.24}$$

Where P_o is the power coupled into the input fibre, α_m is the fibre to fibre optical insertion loss, V_π is the switching voltage and ϕ is a static bias phase shift. This response is shown in Figure 2.6 for a perfectly biased modulator ($\phi = \pi/2$).

By choosing a bias voltage such that $\phi = \frac{\pi}{2}$, then

$$P_m = \frac{P_o}{2}\alpha_m \left[1 - \sin\left(\frac{\pi V_{in}}{V_\pi}\right)\right]$$

$$\approx \frac{P_o}{2}\alpha_m \left[1 - \frac{\pi V_{in}}{V_\pi}\right] \tag{2.25}$$

for $V_{in} << V_\pi$. Thus the modulator has a linear response for small V_{in}. The d.c. term is not of interest, and so the useful power incident on the photodiode is

$$P_{pd} = \frac{\pi P_o \alpha_m \alpha_T V_{in}}{2V_\pi} \tag{2.26}$$

which, following Equation 2.6a and Equation 2.7, gives for the RF output power

$$P_{out} = \left(\frac{\pi \Gamma P_o \alpha_m \alpha_T}{2V_\pi} \frac{R_o}{R_o + R_o} V_{in}\right)^2 R_L \tag{2.27}$$

Since the input voltage is related to the actual RF input power to the module by

$$V_{in}^2 = \left(1 - |\Gamma|^2\right) P_{in} R_{in} = \sigma_{TX} P_{in} R_{in} \tag{2.28}$$

the link gain ρ_G for an externally modulated link can be written

$$\rho_G = \left(1 - |\Gamma|^2\right) R_{in} R_L \left(\frac{r \pi P_o \alpha_m \alpha_T}{2V_\pi}\right)^2 \left(\frac{R_o}{R_o + R_L}\right)^2 \sigma_{RX} \qquad (2.29a)$$

or

$$\rho_G = R_{in} R_L \left(\frac{r \pi P_o \alpha_m \alpha_T}{2V_\pi}\right)^2 \left(\frac{R_o}{R_o + R_L}\right)^2 \sigma_{TX} \sigma_{RX} \qquad (2.29b)$$

The link insertion loss is then defined by Equation 2.8b.

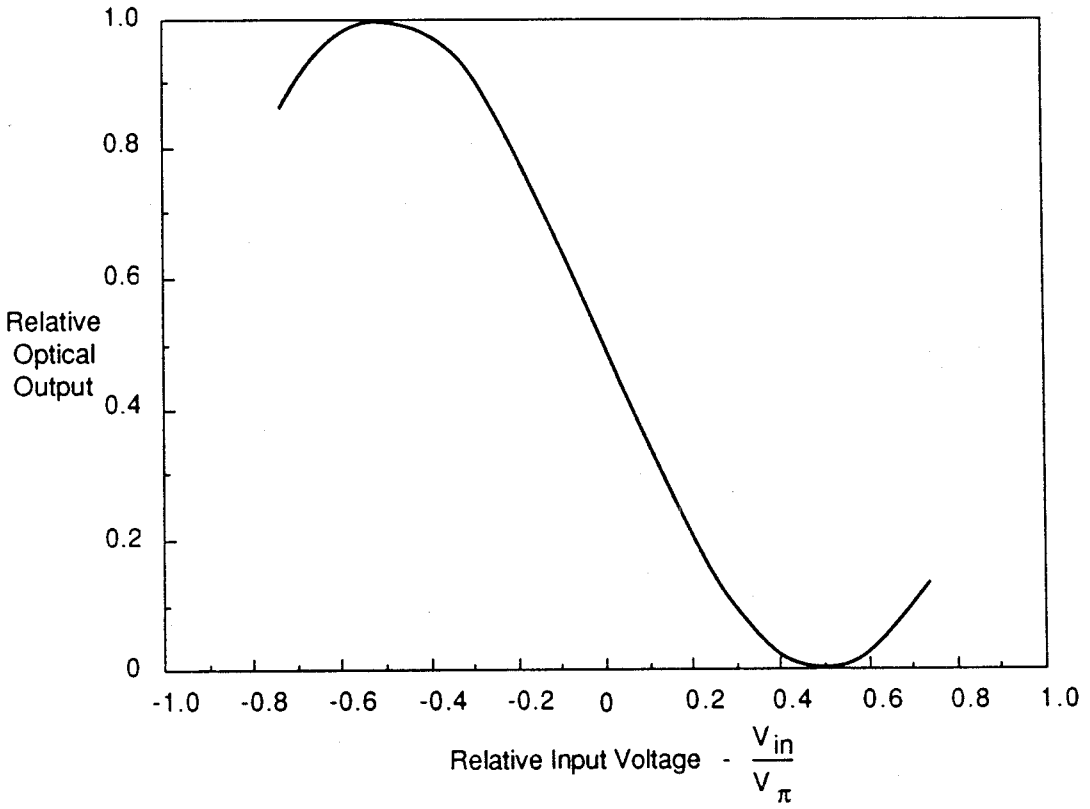

Figure 2.6 Modulator optical output power vs relative input voltage.

It is convenient for comparison purposes later in this report to define a system denoted "E1" by the system parameters for a commercially available 18 GHz modulator (Ref 18) and typical values for laser diode output power and photodiode responsivity, ie

System E1 Specifications (Commercial 18 GHz Link)

P_o = 5 mW

$R_o = R_L = R_{in} = 50\ \Omega$

r = 0.7 mA/mW

α_m = - 6.0 dB = 0.251

V_π = 12 V

σ_{TX} = σ_{RX} > 10 dB, so as an estimate use $\sigma_{TX} = \sigma_{RX} = 0.95$

then putting $\alpha_T = 1$ gives an electrical link loss of

$$\rho_L = 51.3 \text{ dB} \tag{2.30}$$

Equations 2.29 suggest several obvious techniques to improve the insertion loss. These include

(1) decreasing V_π

(2) decreasing α_m

(3) increasing P_o

(4) improving impedance matching to modulator and diode

To illustrate the effect of these changes a system denoted "E2" is specified, using the characteristics of a 40 GHz device demonstrated by Dolfi et al (Ref 16). A higher power laser diode, a perfect impedance match to 50 Ω on the input ($|\Gamma| = 0$) and output are assumed. The system E2 specifications are:

System E2 Specifications (40 GHz Link)

P_o = 30 mW

$R_{in} = R_o = R_L = 50\ \Omega$

r = 0.7 mA/mW

α_m = - 3.5 dB = 0.447

V_π = 7.5 V

$\sigma_{TX} = \sigma_{RX} = 1$

giving an electrical insertion loss of

$$\rho_L = 26 \text{ dB} \tag{2.31}$$

If a device similar to that used in system E2 (which employed a novel aperiodic "Barker code" electrode structure (Ref 16, 20, 21)) was constructed to operate with a 20 GHz bandwidth, it would, from simple geometrical considerations, have a switching voltage reduced to about 4 V. If the delivered optical power is 30 mW, the corresponding insertion loss would only be ≈ 20 dB. There would, however, be a trade-off with increased optical and microwave loss due to the longer device length.

The optical power that can be delivered to the device is limited by photorefractive damage to the electro-optic material and, if single-mode fibre is used at the input, the onset of non-linear processes in the input fibre. The problem of photorefractive damage is severe at visible wavelengths, however, at the preferred communications wavelengths of 1.3 μm and 1.55 μm the problem is drastically reduced. For example, while 3.2 μW of power at 850 nm can cause photorefractive damage, it requires > 0.5 mW at 1300 nm and > 75 mW at 1500 nm (Ref 22). Techniques such as MgO doping (Ref 23) can also be used to reduce photorefractive damage.

2.3.4 Noise in an Externally Modulated Link

The noise contributions to an externally modulated link are identical to those for the directly modulated link. A fundamental and important difference however is that the laser is running cw and can, if required, be actively stabilised. Therefore, the relative intensity noise of the laser can be made negligibly small - a typical value would be -160 dBm/Hz (Ref 1). The thermal and shot noise contributions, given by Equations 2.17 and 2.19, are thus the major limitations to the link sensitivity, the modulator itself being a noiseless device that will only reflect the input noise due to any RF pre-amplification used.

Using the specifications of system E1, the equivalent input noise contributions would be

$$EIN_{TH}^{E1} = -122.6 \text{ dBm/Hz} \qquad (2.32a)$$

$$EIN_{S}^{E1} = -126.3 \text{ dBm/Hz} \qquad (2.32b)$$

indicating that the link will be limited by thermal noise. The results for system E2 are

$$EIN_{TH}^{E2} = -147.7 \text{ dBm/Hz} \qquad (2.33a)$$

$$EIN_{S}^{E2} = -141.1 \text{ dBm/Hz} \qquad (2.33b)$$

In this case the link is found to be shot noise limited, due to the higher optical power incident on the photodiode (in the case of an externally modulated link, $\bar{P}_{pd} = \frac{P_o}{2} \alpha_m \alpha_T$).

Figure 2.7 shows a comparison of the insertion loss and noise contributions for system E2 as a function of the optical input power P_O. Also shown for comparison is the laser EIN of a typical commercially available directly modulated link.

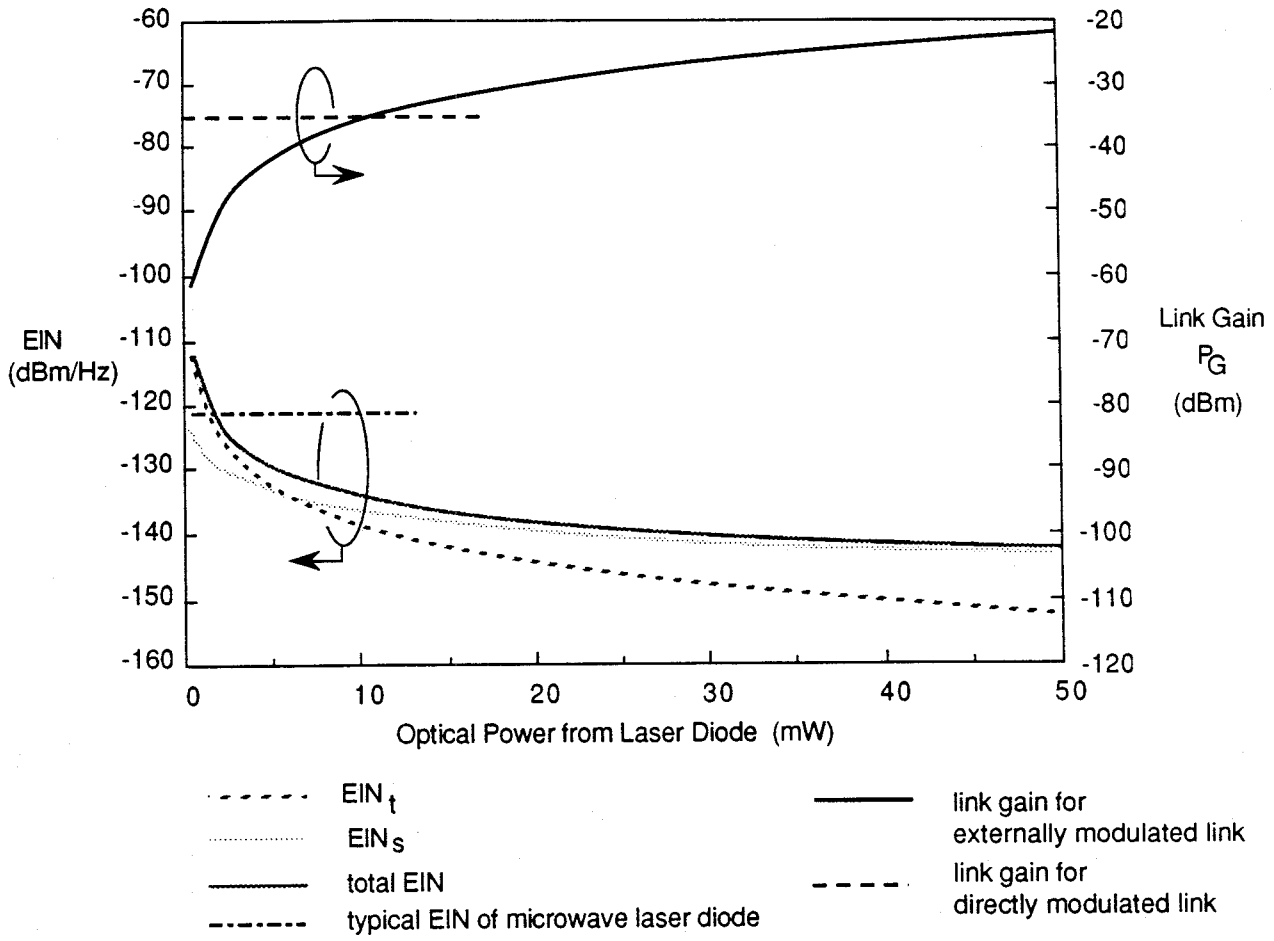

Figure 2.7 Small signal link parameters for system E2.

2.3.5 Modulator Non-Linearity

One of the major disadvantages to using an integrated optical modulator lies in the fact that the modulator response is non-linear. Recalling Equation 2.24

$$\overline{P}_m = \alpha_m P_o \cos^2\left[\frac{\pi V_{in}}{2V_\pi} + \frac{\phi}{2}\right] \tag{2.34}$$

It is clear that any error in the biasing of the modulator will also affect the level and nature of the harmonics. Assuming an error ε in the phase bias, ie $\phi = \frac{\pi}{2} + \varepsilon$, then Equation 2.34 can be written as

$$P_m = \frac{P_o \alpha_m}{2}\left[1 - \sin\left(\frac{\pi V_{in}}{V_\pi} + \varepsilon\right)\right] \tag{2.35}$$

The voltage generated across the load R_L from the photodiode output module is then

$$V_{out}(t) = k\left[1 - \sin\left(\frac{\pi V_{in}(t)}{V_\pi} + \varepsilon\right)\right] \tag{2.36}$$

where

$$k = \frac{1}{2}\left(\frac{R_o R_L}{R_o + R_L}\right) r P_o \alpha_m \alpha_T \tag{2.37}$$

and

$$< V_{in}^2(t) > = \frac{1}{2}\left(1 - |\Gamma|^2\right) P_{in} R_{in} = \frac{1}{2} \sigma_{TX} P_{in} R_{in} \tag{2.38}$$

where < > denotes average over many cycles of the RF input.

To determine the magnitude of the higher order non-linearities, the sinusoidal response of Equation 2.36 must be expanded as a Maclaurin series in V_{in} (Ref 24), ie

$$V(t) \approx k\left[1 - V_s(0) - \sum_{n=1}^{\infty} \frac{1}{n!}\left(\frac{\partial^n V_s(t)}{\partial V_{in}^n(t)}\right)_{V_{in}(t)=0} V_{in}^n(t)\right] \tag{2.39}$$

where

$$V_s(t) \equiv \sin\left(\frac{\pi V_{in}(t)}{V_\pi} + \varepsilon\right) \tag{2.40}$$

Carrying out the differentiation yields

$$V(t) \approx k\left[1 - \sin\varepsilon - \left(\frac{\pi}{V_\pi}\right)\cos\varepsilon\, V_{in}(t) + \frac{1}{2}\left(\frac{\pi}{V_\pi}\right)^2 \sin\varepsilon\, V_{in}^2(t) + \frac{1}{6}\left(\frac{\pi}{V_\pi}\right)^3 \cos\varepsilon\, V_{in}^3(t) + \text{higher order terms in } V_{in}^n(t)\right] \tag{2.41}$$

From Equation 2.41 it is apparent that for a perfectly biased modulator, $\varepsilon = 0$, only odd harmonics contribute to the non-linear response (as expected from Equation 2.35). The output from the modulator for any arbitrary $V_{in}(t)$ can now be calculated using Equation 2.41.

It is usual for broad-band systems to use the input signal

$$V_{in}(t) = V_{in}(\sin\omega_1 t + \sin\omega_2 t) \tag{2.42}$$

to characterise the response. Substituting Equation 2.42 into Equation 2.41 yields terms of the form

$$V_{in}^2(t) = V_{in}^2\left\{\frac{1}{2}(1 - \cos 2\omega_1 t) + \cos(\omega_1 - \omega_2)t - \cos(\omega_1 + \omega_2)t + \frac{1}{2}(1 - \cos 2\omega_2 t)\right\}$$

and

$$V_{in}^3(t) = V_{in}^3\left\{\frac{9}{4}(\sin\omega_1 t + \sin\omega_2 t) - \frac{1}{4}(\sin 3\omega_1 t + \sin 3\omega_2 t) - \frac{3}{4}(\sin(\omega_2 - 2\omega_1)t + \sin(\omega_1 + 2\omega_2)t) + \sin(\omega_1 - 2\omega_2)t + \sin(\omega_2 + 2\omega_1)t\right\}$$

which lead to contributions proportional to ($\omega = \omega_{1,2}$)

fundamental: $$k\cos\varepsilon\left[3K^3 - 2K\right]\sin\omega t \tag{2.43a}$$

second harmonic: $kK^2 \sin\varepsilon \cos 2\omega t$ (2.43b)

third harmonic: $\frac{kK^3}{3} \cos\varepsilon \sin 3\omega t$ (2.43c)

intermods: $2kK^2 \sin\varepsilon \cos(\omega_1 \pm \omega_2)t$ (2.43d)

$\frac{4}{3}kK^3 \cos\varepsilon \sin(\omega_1 \pm 2\omega_{2,1})t$ (2.43e)

where $K \equiv \pi V_{in}/2V_\pi$, and an unimportant d.c. bias term has been omitted.

The average power of each harmonic is

$$\langle P_\omega \rangle = \frac{k^2[3K^3 - 2K]^2 \cos^2\varepsilon}{2R_L} \quad (2.44a)$$

$$\langle P_{2\omega} \rangle = \frac{k^2 K^4 \sin^2\varepsilon}{2R_L} \quad (2.44b)$$

$$\langle P_{3\omega} \rangle = \frac{k^2 K^6 \cos^2\varepsilon}{18R_L} \quad (2.44c)$$

$$\langle P_{int} \rangle = \begin{cases} \frac{2k^2 K^4 \sin^2\varepsilon}{R_L} & (2.44d) \\ \frac{8k^2 K^6 \cos^2\varepsilon}{9R_L} & (2.44e) \end{cases}$$

Equation 2.44a reduces to Equation 2.27 for $K << 1$ and $\varepsilon = 0$ (there is a factor of $\frac{1}{2}$ difference due to Equation 2.44a representing the average power rather than the instantaneous power).

Equation 2.27 is the small signal transfer function, Equation 2.44a is the more accurate large signal transfer function (the form of $< P_\omega >$ is slightly different in the case of a single input tone).

In a narrow band communications oriented system it is usually the intermodulation product at $\omega_{1,2} \pm 2\omega_{2,1}$ that determines the level of harmonic distortion, since all other intermodulation products lie outside the band of interest. In the EW scenario however, where the input frequency is unknown and very large bandwidth coverage is usually required, the level of harmonic distortion, and hence system dynamic range, is determined by the largest of Equations 2.44 ie the noise due to the non-linear "distortion" terms is given by

$$\langle P_{dist} \rangle = \max\{\langle P_{(2)} \rangle, \langle P_{(3)} \rangle\} \quad (2.45)$$

where $<P_{(2)}>$ is the maximum average power in the distortion products due to second order terms (Equations 2.44b, 2.44d), and $<P_{(3)}>$ is the maximum average power in the distortion products due to third order terms (Equation 2.44e).

There are several methods to determine the dynamic range. The usual large signal definition (Ref 7) would entail plotting Equation 2.44a as a function of $<P_{in}>$ (Equation 2.28), and determining the 1 dB compression point. The large-signal dynamic range is then given by Equation 2.23. Alternatively, both $<P_{\omega}>$ and $<P_{(3)}>$ could be plotted as a function of $<P_{in}>$, and the intercept point determined. Once this third-order intercept is known, the usual small-signal spurious free dynamic range can be calculated from Equation 2.22.

The most general and stringent definition of dynamic range (Ref 24) is to equate $<P_{dist}>$ defined by Equation 2.45 to the link noise referred to the output of the photodiode module and determine the corresponding $< P_{in}>$. The value of $<P_{in}>$ defines the upper limit for the input power, P_{max}. The dynamic range is then

$$D.R. = 10 \log \left(\frac{P_{max}}{P_{min}} \right) \tag{2.46}$$

where P_{min} is the link noise referred to the input, as given by Equations (2.17) and (2.19). If third-order distortion terms dominate, this process is equivalent to calculating the SFDR, Equation 2.22. Figures 2.8 and 2.9 show the harmonic response and dynamic range for systems E1 and E2 when they are perfectly biased ($\varepsilon = 0$). For a 40 MHz detection bandwidth, the system sensitivity and dynamic range are

$$S_{E1} = -45 \text{ dBm} \tag{2.47a}$$

$$SFDR_{E1} = 49 \text{ dB} \tag{2.47b}$$

$$S_{E2} = -64 \text{ dBm} \tag{2.48a}$$

$$SFDR_{E2} = 60 \text{ dB} \tag{2.48b}$$

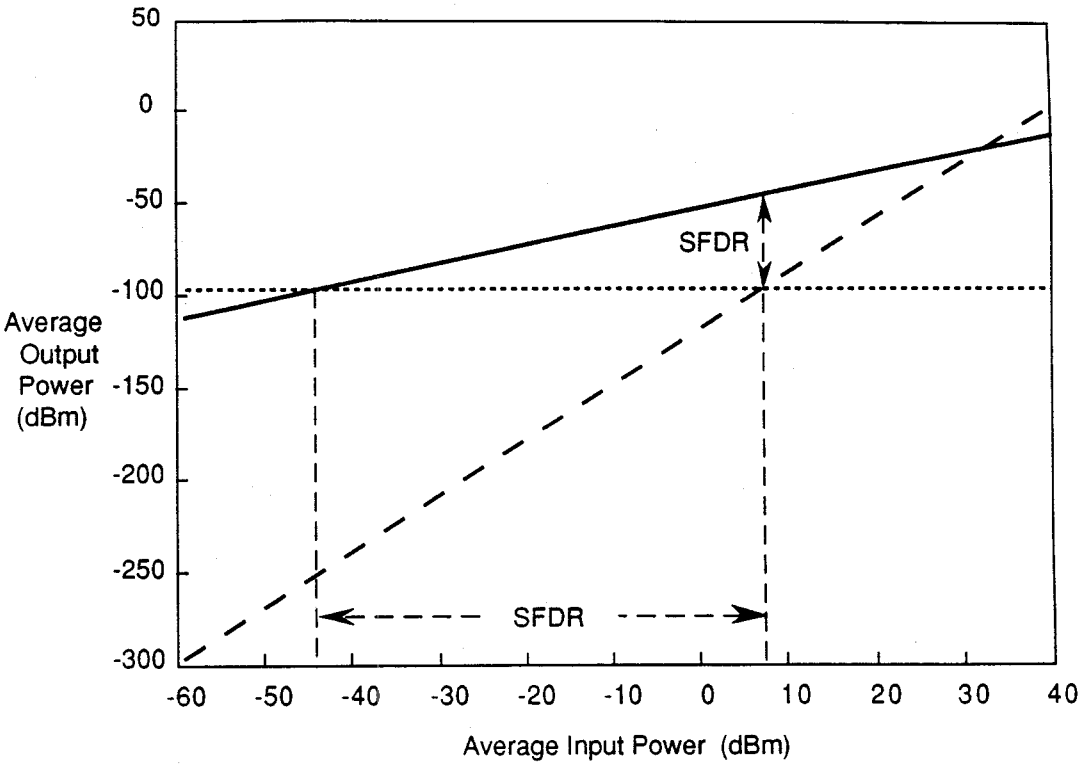

Figure 2.8 Dynamic range calculation for system E1.

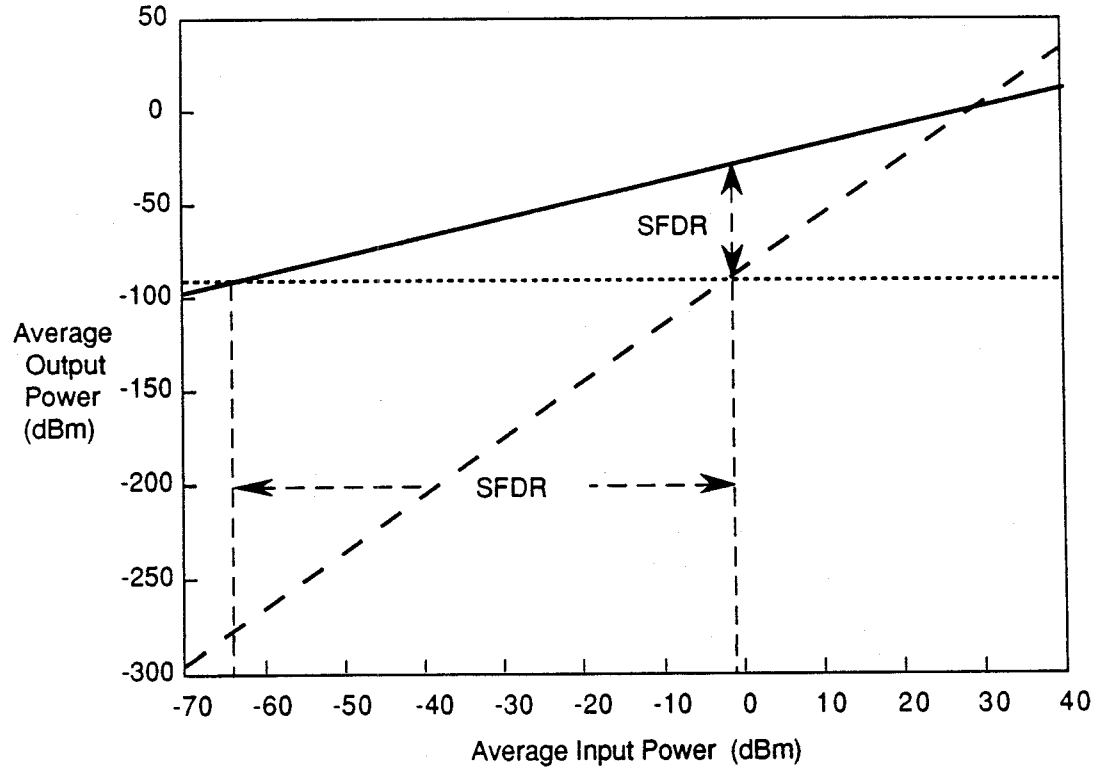

Figure 2.9 Dynamic range calculation for system E2.

If the biasing is imperfect, the second harmonics will be greater than the third-order distortion terms when

$$k^2 K^4 \sin^2 \varepsilon \rangle k^2 K^6 \cos^2 \varepsilon$$

ie

$$\begin{aligned} &\tan|\varepsilon| \rangle |K| \\ &\Rightarrow |\varepsilon| \rangle \left|\frac{\pi V_{in}}{2V_\pi}\right| \end{aligned} \tag{2.49}$$

Equation 2.49 implies that for very small input powers, the phase biasing must be extremely accurate in order for the second harmonic to be less than the usual third-order terms. This is demonstrated in Figure 2.10, which shows the relative magnitude of the second and third-order distortion product powers as a function of phase error for input powers of 0 dBm and -5 dBm into system E2.

The importance of the second harmonic in system terms is significantly decreased however, due to the fact that the third-order terms usually dominate by the time the level of the distortion products reaches that of the link noise. This is demonstrated in Figure 2.11, which shows the effect of a 10° phase error in the biasing of system E2. The dynamic range has been decreased to about 54 dB, a decrease of 7 dB in link performance.

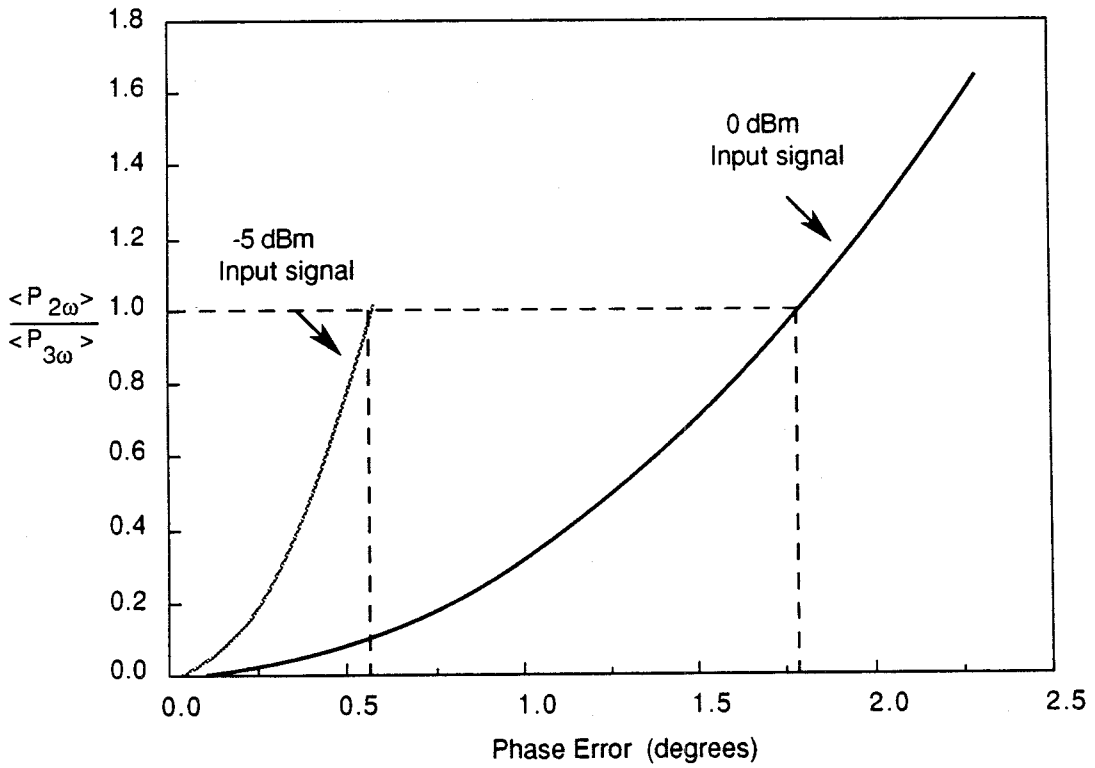

Figure 2.10 Dependence of dominant non-linearity on phase error.

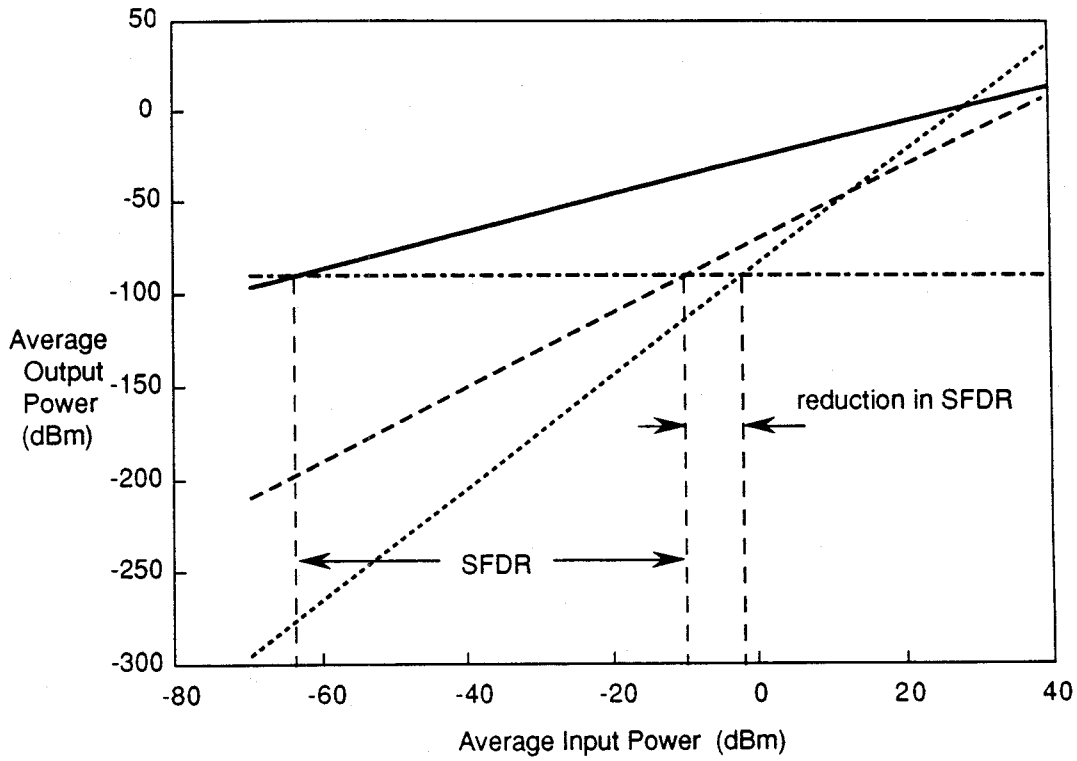

Figure 2.11 Dynamic range calculation for E2 with 10° phase error.

2.4 A Comparison of Link Architectures

2.4.1 Introduction

In this section a comparison is made between the usefulness of direct and external modulation techniques as applied to an EW scenario, and the impact that the limitations of each architecture have on research directions for Electronic Warfare Division is discussed.

A comparison between the performance characteristics of each system architecture can only be made in the light of the requirements imposed on that system by the scenario in which it must operate. In a generic EW scenario, the fundamental operational requirements are, in order of importance,

(1) maximum bandwidth

(2) maximum sensitivity

(3) maximum dynamic range.

Similarly, allocation of research resources must address these same parameters by asking the question, "Will the result of this research lead to significant improvement in the operational performance of the system?" It is inappropriate to allocate research resources to the improvement of system parameters that have only a marginal effect on the practical utility of the system.

In the following sections, the different link architectures will be discussed in terms of these considerations.

2.4.2 Bandwidth

It is clear that external modulators are capable of significantly larger bandwidths than direct modulation can achieve. Of the available commercial devices, only external modulation (Ref 18) is currently capable of covering the traditional 18 GHz EW region of interest. Furthermore, only external modulators have the demonstrated capability of covering the increasingly important region extending from 20 GHz to 40 GHz (Ref 15,16). More importantly, in terms of the criteria discussed in Section 2.4.1, the 40 GHz system (system E2) has a sensitivity and dynamic range that would be useful (though far from ideal) in many EW scenarios. Unfortunately, the same cannot be said of the extremely wide-bandwidth 110 GHz device demonstrated by Nees et al (Ref 17), due to the excessively large switching voltage of $V_\pi = 288$ V, however the potential for operational bandwidths of several hundred gigahertz is apparent.

In terms of potential research directions for photonics in Electronic Warfare Division, the fundamental difference between direct and external modulation schemes is that the technological capability and expertise exists within Australia to undertake research into microwave and millimetre wave external integrated optic modulators. While in principle the physical resources (MBE machines etc) exist within Australia to undertake fundamental research into high-speed laser diode devices, the overwhelming resources and (particularly) experience of countries such as Japan and the USA means that it would be extremely difficult to achieve substantial research breakthroughs in this field.

2.4.3 Sensitivity

The sensitivity of the link is determined by noise contributions and insertion loss. For a directly modulated link, the major limiting factor was demonstrated to be the laser EIN. This implies that any post-transduction techniques for minimising link insertion loss - such as improved impedance matching or amplification (either all-optical within the fibre or conventional post-detection amplification) - will be of limited benefit for a link designed to operate in the generic EW scenario, since the limiting factor is the noise in the transducer itself. The commercial system denoted D1 (Ref 5,6) is an example where the fundamental sensitivity is ~ -45 dBm for a 40 MHz detection bandwidth. As demonstrated in Section 2.2.4.4, improving electrical parameters such as the impedance match of the photodiode will have no effect on this fundamental limit - signals with power levels of less than -45 dBm will still be undetectable.

These considerations imply that useful research directions for improving the sensitivity performance of directly modulated fibre-optic RF links are

(1) development of wide-band, low-noise, high-gain microwave amplifiers for pre-amplification prior to transduction to the optical domain, and

(2) techniques for reduction of laser EIN.

Point number (1) is completely compatible with current general research interests of Electronic Warfare Division and illustrates the close interdependence of both millimetre wave and optical RF technologies. Point number (2) can be approached by either looking at the fundamentals of high-speed laser diode operation, or by use of external techniques to reduce laser EIN.

For the reasons outlined in the previous section, the potential for usefully contributing to the improvement of the physical parameters of high speed semiconductor laser diodes using Australian facilities is limited. This leaves the option of external techniques. The advantage of improved impedance matching to the laser has been demonstrated by the performance of system D2 of Section 2.2.4.4, however a novel optical technique will be described in Section 3 that should simultaneously achieve both reduced RIN and linearisation of the laser response.

In contrast to directly modulated links, externally modulated links will benefit from improvements in link insertion loss, due to the fact that the transducer is a passive device. It was demonstrated in Section 2.3 that the most substantial gains were obtained by reducing the optical loss terms and reducing the switch voltage V_π. Techniques such as cooling the photodetector simply by mounting it on a Peltier cooler would, for example, improve the performance of the commercial 18 GHz system (Ref 18) E1 to a point where the sensitivity was determined by shot noise or ~ -51 dBm for a 40 MHz detection bandwidth. As in the case of a directly modulated link, low-noise, wide-bandwidth pre-amplifiers would also be of substantial benefit. Thus, useful research directions for externally modulated fibre-optic RF links are

(1) development of wide-band, high gain, low noise amplifiers

(2) reduction of link insertion loss via

  (a) low V_π structures

  (b) low optical insertion loss techniques

  (c) low electrical insertion loss techniques.

2.4.4 Dynamic Range

The dynamic range of a fibre-optic RF link is determined by both the sensitivity and by the non-linear response of the RF/optical transducer.

For directly modulated links, it is usual to find the third-order intercept and 1 dB compression point quoted as specifications, however these values are normally determined at frequencies well below ω_r. As indicated in Section 2.2, near $\omega_r/2$ the harmonic distortion products can rise dramatically with, for example, the second harmonic being only 8 dB below the fundamental for a modulation depth of 0.8 at $\omega_r/2$ (Ref 1) . While this is acceptable in a narrow-band communications scenario, it is unacceptable for the generic EW scenario, and clearly the commercial specifications are inadequate to fully characterise the link performance.

External modulators have the advantage that the non-linear response is frequency independent and easily calculated (as is done in Section 2.3.4), and for a perfectly biased modulator only odd harmonics contribute.

Typical dynamic range calculations for systems D1, E1 and E2 have been included in the appropriate sections. It is clear that the achievable dynamic range of external modulators is at least equal to that of directly modulated links. It is also apparent that for both types of links if the non-linear response could be minimised, significant enhancement of the dynamic range would result. A novel technique for achieving this is described in Section 3.

2.4.5 Conclusions

The following summarises the results of Section 2:

(1) the bandwidths achievable by external modulation far exceed those achievable by direct modulation,

(2) the sensitivity of directly modulated links is limited by laser noise. The sensitivity of externally modulated links should ideally be limited by shot noise, however if off-the-shelf components are used thermal noise may dominate

(3) the insertion loss of externally modulated links can be made at least comparable to or less than that of commercially available direct modulation links. Improving the insertion loss of a directly modulated link via post-transduction techniques such as signal amplification and photodiode impedance matching will not improve fundamental system performance, whereas improving the insertion loss of an externally modulated link will do so,

(4) the reduction of transducer non-linearities will improve dynamic range. As will be shown in Section 3, the linearisation of the transducer response is best achieved using external integrated optic modulators,

(5) the development of wide-band, low noise, high-gain microwave amplifiers will be of extreme importance to the development of all types of optical links,

(6) the capability exists within Australia to undertake fundamental design, construction and testing of leading-edge microwave integrated optical components. This capability does not exist in the field of high speed laser diodes, mainly due to a lack of experience and demonstrated expertise in the area of fabrication of such devices.

3 SOME FIBRE-OPTIC LINK APPLICATIONS

3.1 Introduction

In this section some EW scenarios employing the various link architectures are presented and discussed. Two generic EW scenarios are defined and example calculations for link performance in each scenario are given. Section 3.2 introduces the "remote transmitter" scenario, whereas Section 3.3 deals with the "remote receiver" scenario. In both Sections 3.2 and 3.3 the links are specified entirely using off-the-shelf, commercially available products.

Section 3.4 emphasises the potential of integrated optic technology by examining the performance of a link that has parameters chosen from "best performance" laboratory devices that have been reported in the literature. Finally, Section 3.5 examines the limitations of optical transduction techniques and proposes a novel solution for reduction of both laser noise and non-linear device response.

3.2 The "Remote Transmitter" Scenario

In the remote transmitter scenario, the assumption is made that only basic (or no) signal pre-amplification and little (or no) signal pre-processing is available before transduction to the optical domain. It is assumed that the more sophisticated processing and amplification takes place at the receiver end of the link. An example of such a scenario would be the EW mast of a submarine, where there is little room for extraneous electronics. The proposed link architecture is shown schematically in Figure 3.1. It is required in this case to maintain as high a sensitivity as possible in the EW bands of interest.

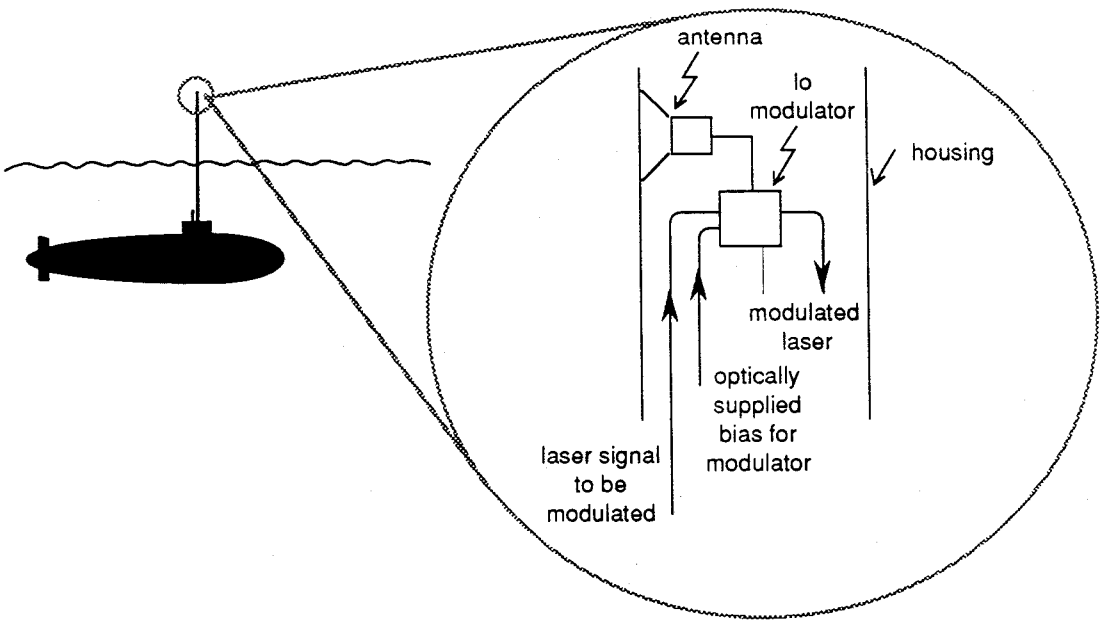

Figure 3.1 Fibre optic architecture for submarine EW mast.

It is clear in this case that an external modulator - with its comparative lack of associated electronics (a small dc bias voltage is all that is required) and lack of laser noise - is the device of choice. The assumed system parameters are:

1. No signal pre-amplification.
2. 20 mW optical power delivered to modulator, $\lambda = 1.5\ \mu m$.
3. 18 GHz bandwidth modulator (Md Y-35-8808-02 (Ref 18)).

   - matched to 50 Ω.

   - $\lambda = 1.5\ \mu m$.

   - $V_\pi = 14$ V.

   - optical insertion loss = 6.0 dB.

   - electrical return loss > 10 dB (assume $\sigma_{TX} = 0.95$).
4. Link length = 1 km.

   - link optical loss, including connectors, 2 dB (optical).
5. 25 GHz bandwidth receiver (Md PDC4304 (Ref 25))

   - matched to 50 Ω.

   - r = 0.95.

   - assume $\sigma_{RX} = 0.95$.
6. No post-amplification is assumed.

This link architecture is of interest because there are no active electronic components associated with either the antenna or the physical link, and thus the system should be

a. very secure,

b. free from electromagnetic "leakage" (ie covert),

c. resistant to electromagnetic interference.

Two different receiver scenarios are specified. The first assumes an IFM receiver is used at the link output, with a detection bandwidth of ~ 100 MHz. The second assumes a scanning super-heterodyne (SH) receiver with a 40 MHz detection bandwidth.

From the theory outlined in Section 2, the system performance is found to be

bandwidth	:	0 - 18 GHz
sensitivity	:	-48 dBm (IFM); -52 dBm (SH)
SFDR	:	52 dB (IFM); 55 dB (SH)
electrical insertion loss	:	42 dB
link noise figure	:	46 dB.

It is interesting to compare the total insertion loss of 42 dB for the 1000 m optical link with that achievable by conventional technology, ie coaxial cable and waveguide. Using the attenuation figure of 1.46 dB/m (Ref 1) for a 10 GHz signal propagating down standard RG-402U semi-rigid coaxial cable, it is found that 42 dB corresponds to about 30 m of propagation. A similar calculation for aluminium rectangular waveguide (WR-90) (Ref 1) with an attenuation of 0.13 dB/m at 12.4 GHz yields an equivalent propagation length of ~ 330 m.

If an improvement in link performance is required, broad-band amplification at the antenna is necessary. The effect of adding pre-amplification stages can be determined by treating the link as a "black-box" with a gain of -42 dB and a noise figure of 46 dB, and using Frii's formula (Ref 1) to calculate the new overall gain and noise figure.

If the bandwidth is restricted to the 6 - 18 GHz region, a good amplifier to use would be the WJ-6885-816 cascaded amplifier package (Ref 26), which has a gain of 36 dB and a noise figure of 5.5 dB.

From Frii's formula, the overall link gain and noise figure are -6 dB and 11 dB respectively, resulting in a link with the performance specifications:

bandwidth	:	6 - 18 GHz
sensitivity	:	-83 dBm (IFM); -87 dBm (SH)
SFDR	:	52 dB (IFM); 55 dB (SH)
electrical insertion loss	:	6 dB
link noise figure	:	11 dB.

These figures are very acceptable in terms of general EW performance requirements, and are achieved with a minimum of electronic complexity at the antenna.

Having established that a fibre optic link driven by a remoted external modulator is a viable concept using available off-the-shelf technology, it is interesting to pursue the question of application of the technology. The moderate sensitivity (~ -50 dBm) means that the antenna cannot be very far from the emitters - usually an unhealthy situation in a hostile environment. An interesting application however may be a remotely deployable and expendable EW mast for submarines. The modulator , and if necessary pre-amplifiers, could be housed in a buoyant pod

upon which a wide-band antenna (or antenna arrays) would be mounted The pod could be allowed to rise to the surface in order to sample the electromagnetic environment, without the necessity of having the submarine itself exposed to the risks associated with being near the surface. The pod could be winched back down to the submarine after the surveillance period, or if necessary could simply be detached and allowed to sink. The possibilities of more sophisticated pods incorporating lure/decoy modes could also be investigated.

Given that the price of remoting the antenna is mainly in the transduction process, and only about 0.6 dB/km (electrical) penalty is associated with the actual length of the link, there could be substantial advantages for the safety of the submarine which accrue simply through the fact that the actual position of the vessel would be difficult to determine based upon the observation of the EW mast.

3.3 The "Remote Receiver" Scenario

This situation is taken to be the opposite of that described in Section 3.2. It is assumed that the transmitter has available to it any required amount of pre-amplification and signal pre-conditioning necessary, but that the complexity of the receiver end of the link must be minimised. This very specific situation has been included to illustrate a situation where link insertion loss becomes a parameter of fundamental importance.

A typical example of this situation is the case of an airborne towed decoy, in which the receiving antennas etc are situated in the body of the aircraft, and there is a fibre optic link to the decoy, the output of which is re-radiated after amplification by a suitable broadband TWT. This situation is shown schematically in Figure 3.2.

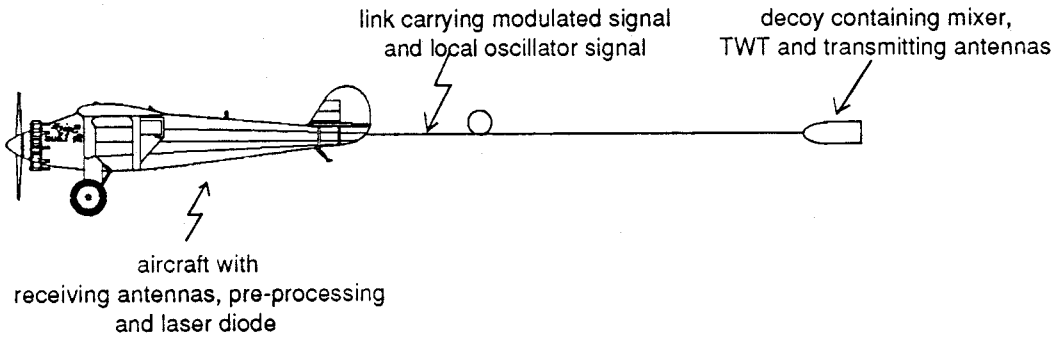

Figure 3.2 Fibre optic architecture for aircraft towed decoy.

Due to the assumption that signal pre-amplification etc is not a problem, and the relatively high input power requirements of a TWT (typically +10 dBm (Ref 27)), the main factor of concern is the link insertion loss, which must be minimised.

In this case, the use of a directly modulated laser diode is the optimal "off-the-shelf" solution, the only difficulty arising due to the limited bandwidth of these devices - of the order of 10 GHz (Ref 5,6). It will therefore be possible to cover only the 8 - 18 GHz band, where the RF input is first downconverted to modulate the laser, and then upconverted again at the decoy. There are any number of suitable wide-band mixers, and so for the sake of simplicity mixer loss will be ignored (this is only significant at the decoy, the assumption being that there is sufficient amplification available prior to the laser diode to achieve appropriate input levels).

A typical output for the TWT's used in airborne decoys would be +50 dBm, and a typical gain is ~ 40 dB (Ref 27). Thus, ~ 10 dBm is required at the input to the TWT. Based on these figures, an off-the-shelf link would consist of

1. directly-modulated laser (eg QLM1300MW-002 (Ref 5)).
   - matched to 50 Ω.
   - RF input ~ +10 dBm.
   - σ_{TX} ~ 0.95.
   - M = 0.04.
   - output power (optical) ~ 1.0 mW.
   - λ = 1.3 μm.
2. link length < 1 km: therefore ignore optical link losses
3. 10 GHz bandwidth detector (eg QDEMW-002 (Ref 5))
   - r = 0.4 mA/mW
4. Mixer to upconvert to 8 - 18 GHz.
5. Single post-amplification stage (eg WJ-6885-816 (Ref 26))
   - gain = 36 dB
   - noise Figure = 5.5 dB

Ignoring mixer losses and using the specified Q-LINK-10 (Ref 5) electrical insertion loss of ~ 35 dB, it is found that the total output power available to the TWT will be ~ + 11 dBm, implying that the concept of having a fibre-optic link to a towed decoy is viable using off-the-shelf technology, providing that a small secondary amplification stage to overcome mixer losses is incorporated. It should be noted that the local oscillator for the mixer in the decoy can also be supplied via an optical link and should be the same oscillator as used in the original down-conversion, thereby maximising the possibility of maintaining the phase coherence of the reproduced signal.

The use of a fibre optic link to a towed decoy becomes more attractive if impedance matching of the laser is employed, since this reduces the insertion loss. Depending upon whether the decoy is expendable or not, and whether the extra cost is justified, impedance matching of the photodiode in the decoy will also substantially reduce insertion loss and reduce post-detection amplification requirements.

The advantages of having a fibre-optic link to the decoy include:

a. reduced channelising of original RF
b. maintain phase coherence of the re-radiated signal
c. lack of electromagnetic leakage from tow cable
d. possibility of avoiding the use of digital RF memory by exploiting the low-loss characteristics of optical delay lines.

3.4 Near-Future Improvements in Link Performance

It is appropriate at this stage to look at the possibilities offered by "state-of-the-art" laboratory devices, to determine their impact on the performance characteristics of fibre-optic RF links for EW.

The most likely devices to offer substantial improvement in commercially available bandwidth coverage will be external modulators. For direct detection links, the Barker-code electrode pattern (Ref 16,20,21) will probably be employed. Thus, bandwidths of 40 GHz are achievable (Ref 16) with switching voltages of V_π = 7.5 V. Optical losses within the modulator depend

strongly upon modulator length, fibre alignment coupling loss, mode-mismatch etc, however losses of the order of 0.3 dB/cm propagation loss and 0.3 dB/interface coupling loss have been achieved (Ref 28). The 40 GHz device demonstrated by Dolfi et al (Ref 16) had an active length of ~ 1 cm, and so it is reasonable to expect such modulators to evolve to a point where the optical insertion loss is as low as ~ 2 - 2.5 dB.

All of the components mentioned in this section have been demonstrated in the laboratory, and as such it is reasonable to expect that they represent the next generation of commercial devices, probably available within 5 years.

A hypothetical link based upon these components would have the following specifications:

1. 40 GHz pre-amplifier: (Ref 29)
   - gain = 13 dB
   - noise figure = 2.5 dB
2. 40 GHz External Modulator (Ref 16)
   - V_π = 7.5 V
   - λ = 1.5 μm
   - optical power input = 10 mW
   - optical insertion loss = 3.0 dB
3. 40 GHz monolithic integrated photodiode and pre-amplifier: (Ref 30)
   - r = 0.9
   - gain = 20 dB
   - noise figure (assumed) ~ 4.0 dB.

Ignoring matching losses into and out of the various modules, the overall link performance for a short optical link would be -

bandwidth	:	0 - 40 GHz
link equivalent input noise	:	- 148 dBm/Hz
link gain	:	0 dB
link noise figure	:	26 dB

For a 100 MHz detection bandwidth, the above figures give a sensitivity of -68 dBm.

Advances in fibre technology indicate that the above figures will be basically unchanged for links less than several kilometres in length. For short propagation distances (where chromatic dispersion is not a problem), pure silica core fibre with shifted cutoff wavelength design already exhibits losses of the order of 0.172 dB/km in mass production (Ref 31). For extremely long links (for delay lines of several hundreds of microseconds for example), special dispersion shifted fibre (dispersion slope at 1550 nm of ~ 0.08 ps/km/nm^2) must be used, however the attenuation penalty rises to 0.21 dB/km (one kilometre corresponds to 5 microseconds delay).

Thus the above calculations indicate that with currently demonstrated technology, a 40 GHz bandwidth fibre-optic RF link could be constructed with the properties of

a. zero insertion loss
b. extremely good sensitivity
c. useful dynamic range.

The limiting factor in the link performance detailed above is the dynamic range, which is restricted due to the non-linear response of the integrated optic modulator. A similar situation exists in the case of directly-modulated laser diodes, whose performance is limited by both non-linearities and excessive laser noise. The next section details a proposal to overcome these problems.

3.5 Reduction of Transducer Non-linearities and Noise

As has been demonstrated in the previous sections, the major factors limiting the usefulness of optical techniques for RF signal processing are transducer non-linearity and, in the case of directly modulated links, excessive laser noise. The solution to these problems is based upon the realization that the end of the transduction process does not necessarily occur when the modulated light leaves the laser diode or the integrated-optic modulator. The unique low-loss properties of optical fibre means that the output can be stored, part of it pre-processed, and some signal correcting can be undertaken prior to final transmission of the modulated signal.

Such an optical "feed-forward" technique has been implemented by researchers at Melbourne University (Ref 32) as a means of attempting to reduce laser RIN. In this section a variant of the technique is proposed which will enable not only a reduction of laser RIN, but removal of non-linear response as well.

The idea is shown schematically in Figure 3.3 for the case of an external modulator.

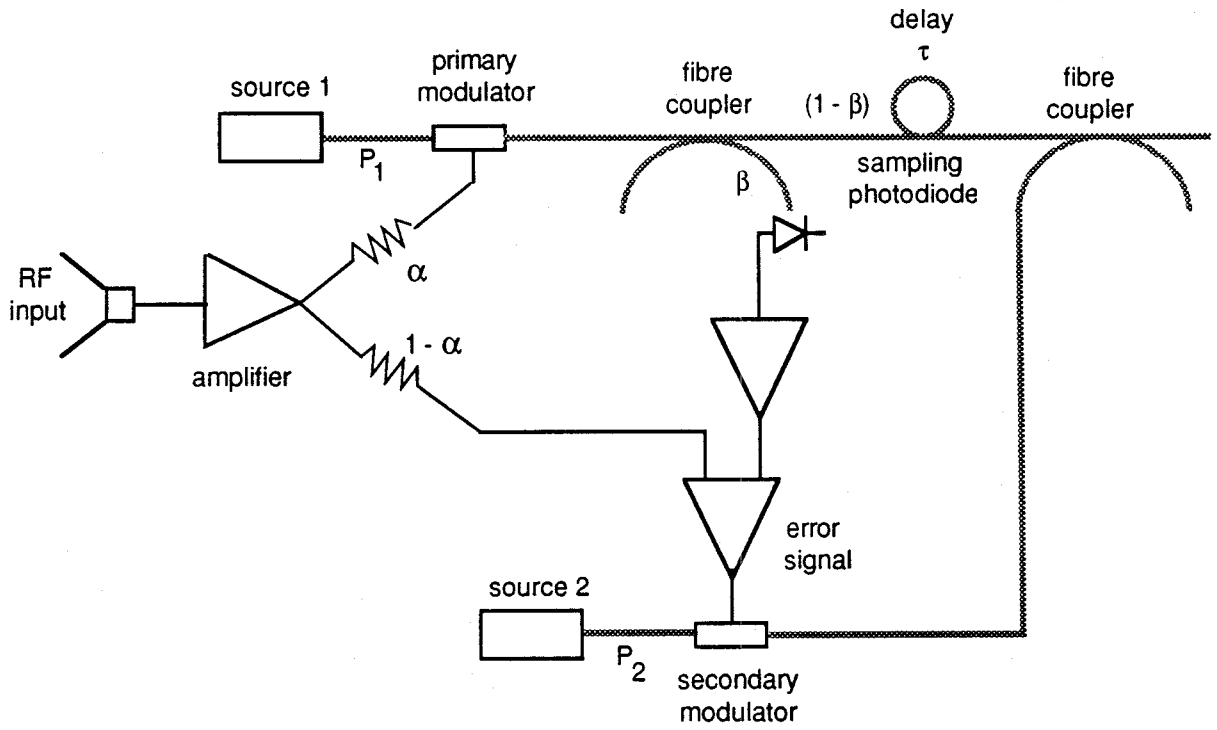

Figure 3.3 Linearisation of integrated optical modulator response.

The incoming RF signal is first amplified an then split into two. One output drives the primary modulator, the output of which is sampled and delayed, as shown. The sample signal on the photodiode is then amplified, compared to the original RF input and an error signal is generated. This error signal drives the secondary modulator. The output from the secondary modulator is added to the delayed version of the output from the primary modulator, via a simple 3 dB coupler. The delay τ is chosen such that the correction signal arrives with the appropriate timing to correct the non-linear response due to the primary modulator.

Since the photodiode responds simply to the sum of the intensities, this procedure will result in linearisation of the total response.

The modulators would ideally be of identical construction and manufactured on the same electro-optic substrate. The linearisation of the response will be particularly good if $P_2 > P_1$, since this will minimise the required error voltage, thereby keeping the secondary modulator in its linear region of operation. The choice of using external modulators rather than laser diodes arises due to the superior bandwidth and essentially noiseless operation of these devices.

By following the signal paths shown in Figure 3.3 the optical response of the system as a function of applied voltage V can be shown to be (assuming 3 dB coupling loss at the output and perfectly chosen delay τ):

$$P_T = \frac{(1-\beta)P_1^{(0)}}{4}\left\{\left[1+\frac{(1-\alpha)}{\alpha A_2}\right] - \sin\left(\frac{\pi(1-\alpha)V}{V_\pi}\right) - \frac{(1-\alpha)}{\alpha A_2}\sin\left(\frac{\pi\alpha A_2 V}{V_\pi} - \frac{\alpha A_2}{1-\alpha}\sin\left[\frac{\pi(1-\alpha)V}{V_\pi}\right]\right)\right\} \quad (3.1)$$

where a small signal analysis gives for the magnitude of the gains A_1 and A_2,

$$A_1 = \frac{-2V_\pi\alpha}{\pi k\beta(1-\alpha)P_1^{(0)}} \quad (3.2)$$

$$A_2 = \frac{(1-\beta)(1-\alpha)P_1^{(0)}}{\alpha P_2^{(0)}} \quad (3.3)$$

where

$$k = \frac{1}{2}\frac{R_o R_L}{R_o + R_L} r\alpha_m^{(1)} \quad (3.4)$$

It is clear from Equation 3.1 that the small signal response is of the form

$$P_T = \frac{(1-\beta)P_1^{(0)}}{4}\left\{\left[1+\frac{(1-\alpha)}{\alpha A_2}\right] - \frac{(1-\alpha)\pi V}{V_\pi}\right\} \quad (3.5)$$

Like the usual small signal response for a single integrated optic modulator, Equation 3.5 consists of an unimportant dc bias term and the linear response (compare Equation 2.25). The fundamental difference lies in the required "small signal" criterion. In Equation 2.26 it is required that the input signal $V << V_\pi$, whereas for Equation 3.5 the requirement is that error signal V_E associated with the deviation from linearity of the response of the primary transducer satisfy $V_E << V_\pi$.

This latter criterion is much less restrictive than that associated with a single transducer.

The highest order correction to Equation 3.5 is a term of the form

$$P_C = \frac{(1-\beta)P_1^{(0)}}{24}\frac{(1-\alpha)}{\alpha A_2}\left\{\frac{\pi\alpha A_2 V}{V_\pi} - \frac{\alpha A_2}{1-\alpha}\sin\left[\frac{\pi(1-\alpha)V}{V_\pi}\right]\right\}^3 \quad (3.6)$$

For $V << V_\pi$ the sine term can be expanded to give

$$P_C \approx \frac{(1-\beta)\,P_1^{(0)}}{5184}\,(\alpha A_2)^2\,(1-\alpha)^7\left(\frac{\pi V}{V_\pi}\right)^9 \tag{3.7}$$

In order to avoid tedious trigonometry, the effect of linearising the transducer response on the dynamic range of an integrated optic modulator will be calculated for a single input tone

$$V_{in}(t) = V_{in} \sin \omega t. \tag{3.8}$$

The normal response would yield a third order non-linearity given by

$$V_{(3\omega)}^{normal} \approx \frac{k}{48}\left(\frac{\pi V_{in}}{V_\pi}\right)^3 (1-\beta)\,P_1^{(0)} \tag{3.9}$$

whereas the linearised response gives

$$V_{(3\omega)}^{linearised} \approx \frac{k}{5184}\,(1-\beta)\,P_1^{(0)}\,(\alpha A_2)^2\,(1-\alpha)^7\left(\frac{\pi V_{in}}{V_\pi}\right)^9 \cdot \frac{21}{64} \tag{3.10}$$

The average power is just

$$\left\langle P_{(3\omega)}^{normal}\right\rangle = \frac{k^2}{4608}\left(\frac{\pi V_{in}}{V_\pi}\right)^6 \frac{\left[(1-\beta)\,P_1^{(0)}\right]^2}{R_L} \tag{3.11}$$

$$\left\langle P_{(3\omega)}^{linearised}\right\rangle = \frac{441\,k^2\left[(1-\beta)\,P_1^{(0)}\right]^2}{(331776)^2}\,\frac{(\alpha A_2)^4\,(1-\alpha)^{14}}{R_L}\left(\frac{\pi V_{in}}{V_\pi}\right)^{18} \tag{3.12}$$

Figure 3.4 shows both the normal response and the effect of linearising the response for two identical modulators with identical optical input powers. Figure 3.5 highlights the effectiveness of the scheme by showing the normal and linearised response obtained from a highly overdriven modulator (ie the maximum input voltage $V_{in}>V_\pi$). The improvement in dynamic range obtained from the feed-forward linearisation, of the order of 15 dB, is shown in Figure 3.6.

Figure 3.7 shows a similar feed-forward architecture to linearise and reduce the RIN of a laser diode - a design which could usefully augment the performance of high speed laser diode transmitters.

Figure 3.8 shows an architecture to minimise the noise of a conventional CW laser (this is effectively an electro-optic "noise-eater" configuration, somewhat similar to acousto-optic noise-eaters employed in several commercial laser systems, however it employs feed-forward error correction). This architecture could be particularly useful for reducing the low frequency RIN associated with certain solid-state lasers. Since the RIN has only low frequency components, a lumped element modulator could be used, thereby reducing design complexity and cost.

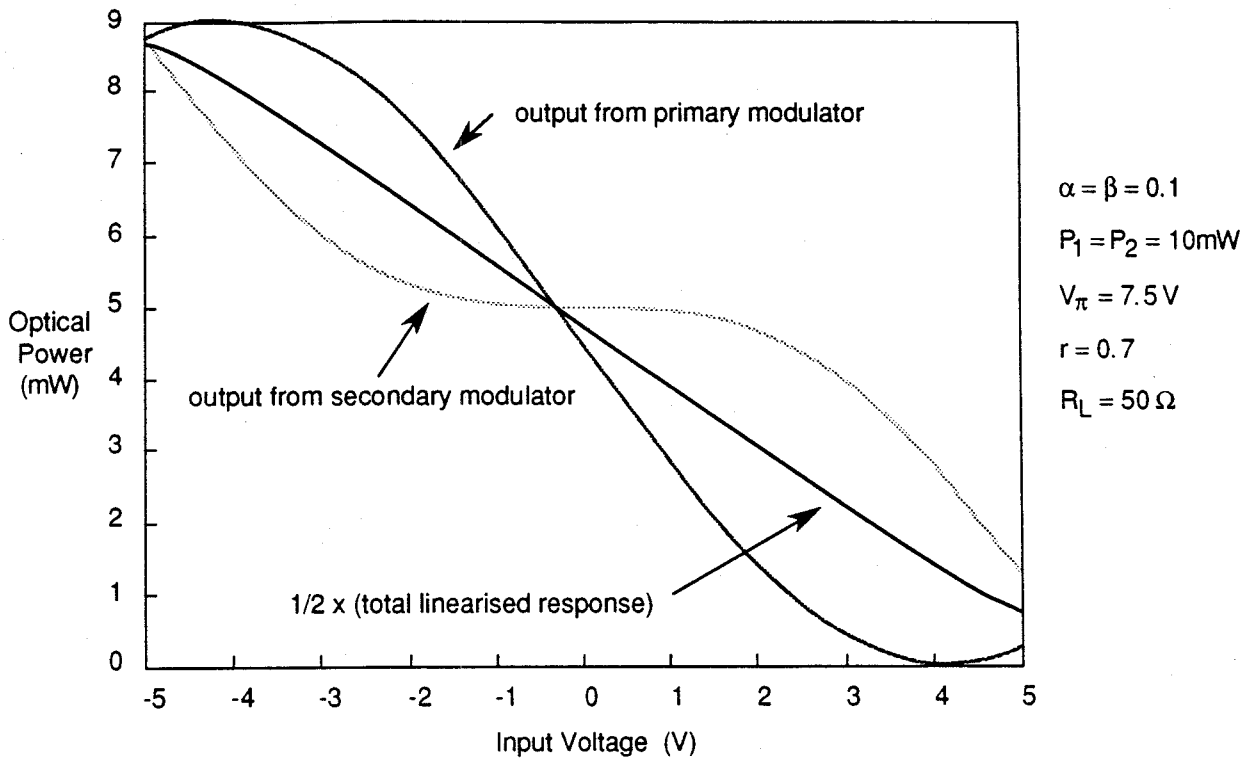

Figure 3.4 Linearisation modelling results.

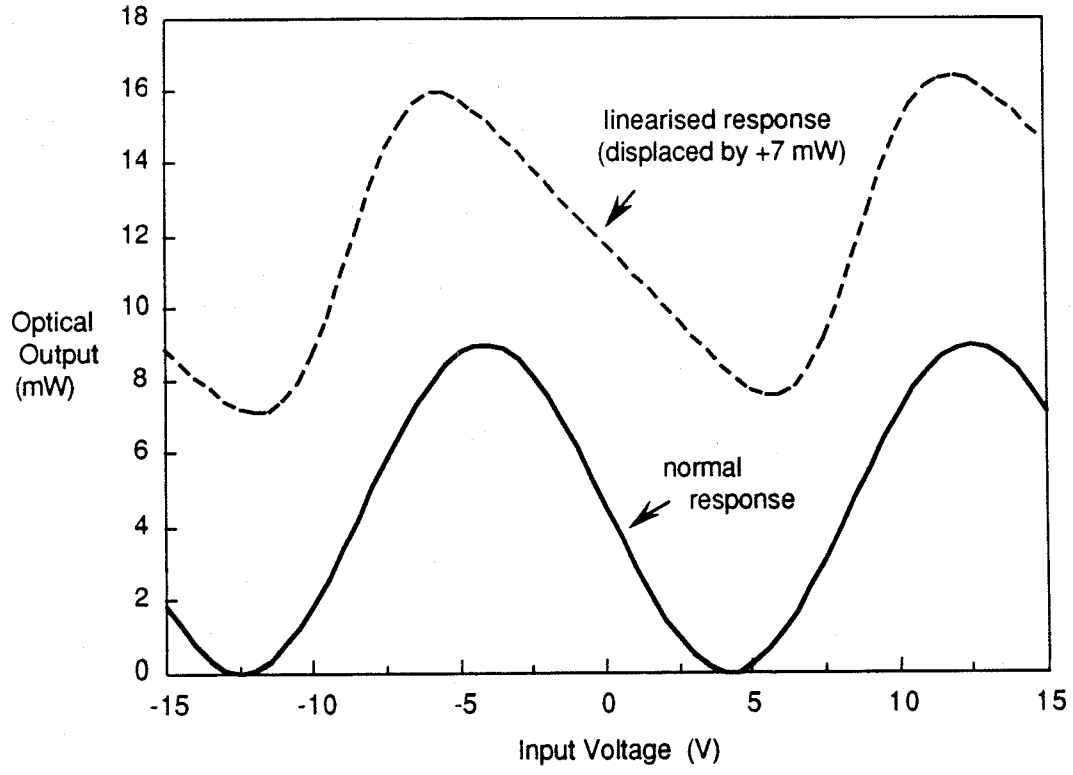

Figure 3.5 Linearisation modelling results.

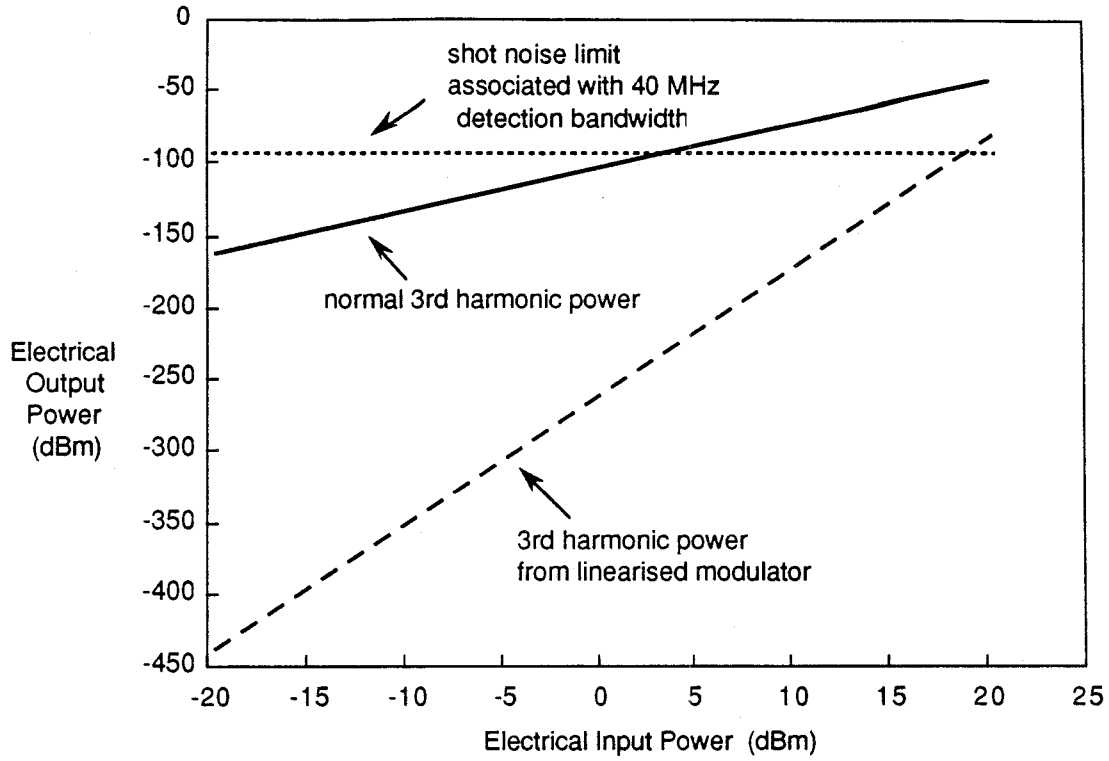

Figure 3.6 Improvement in single tone dynamic range due to feed forward linearisation.

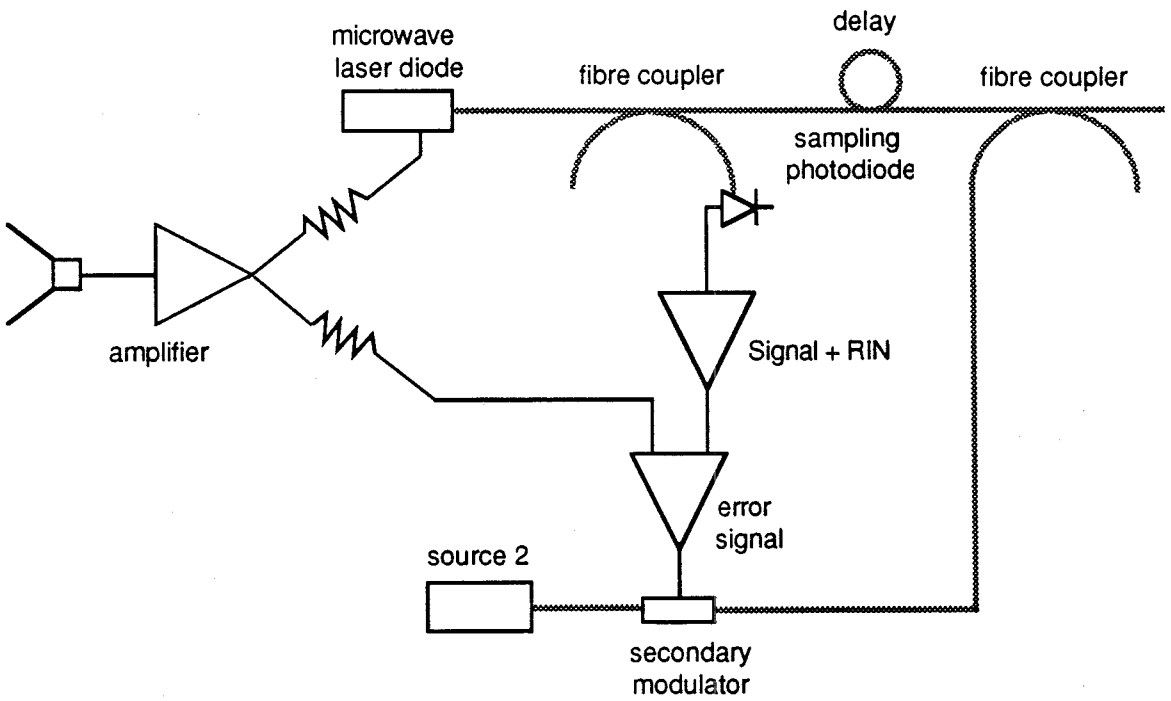

Figure 3.7 Linearisation of laser diode response and reduction of RIN.

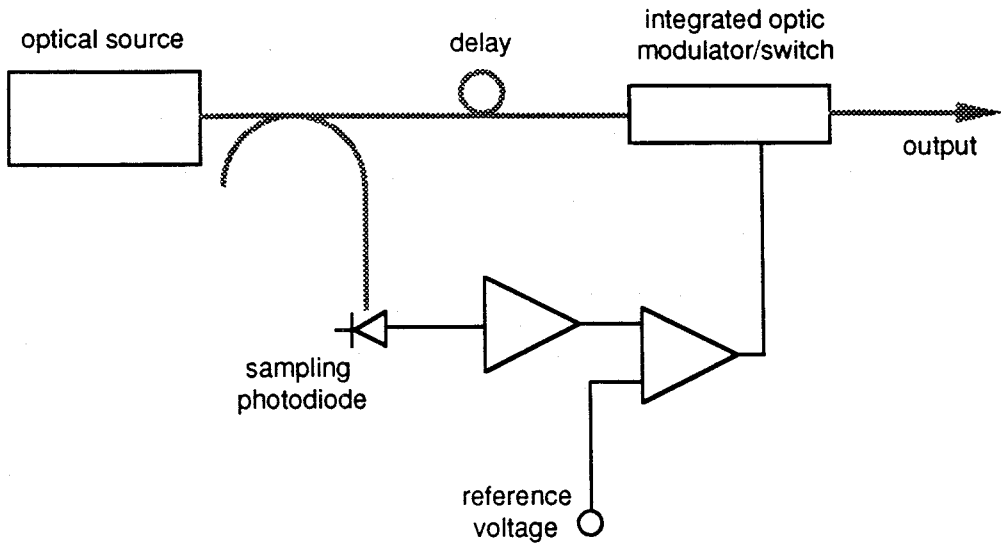

Figure 3.8 Electro-optic "noise-eater" using feed-forward architecture.

The 3 dB coupling loss implied at the outputs of Figures 3.3 and 3.7 can be avoided if two different laser sources of wavelengths λ_1 and λ_2 are used for the primary and secondary modulators respectively. Wavelength division multiplexing can then be used to combine the signals without the 3 dB optical (6 dB electrical) penalty, thereby increasing the electrical power delivered at the end of the link by 6 dB. The difference in photodiode responsivity at each wavelength is easily compensated by increasing or decreasing the intensity of the optical correction signal appropriately.

It is clear that for very high speed operation the delay τ must be very accurately set, which presents a major difficulty in terms of device reproducibility and ease of manufacture. This difficulty can be overcome by extending the feed-forward concept to the realisation that the error signal need only have the correct timing at the photodiode. This suggests that if different wavelengths λ_1 and λ_2 are used, the delay τ and the propagation length L can both be exploited to ensure correct timing of the error signal due to the different propagation times experienced by the two wavelengths. Since the two modes evolve quite slowly relative to one another, very accurate timing should be achievable. The low loss of the fibre means that it is not significant if an extra few tens of metres must be added to the link to ensure exact timing. Alternatively, if the link length cannot be varied, then both lasers could be actively wavelength stabilised and one of them subsequently tuned (for example by temperature tuning or varying the cavity length) to achieve near perfect timing of the correction signal. Using this technique thus enables high speed operation and simultaneously avoids the 3 dB coupling loss penalty discussed previously.

In conclusion, the proposed feed-forward architectures have the potential to increase the utility of RF fibre-optic links by substantially increasing the linearity and decreasing noise contributions, thereby increasing the dynamic range and sensitivity of both direct and externally modulated links. Since they are optical solutions, any improvement contributes as the square in the electrical domain.

Finally, it is to be noted that the technology and expertise exists within Australia to construct proof of concept devices for practical evaluation.

4 DELAY LINE SIGNAL PROCESSING - THE OPTICAL IFM

4.1 Introduction

While fibre-optic links are useful for many applications, it would be desirable to extend their utility and exploit the advantages of working at optical frequencies by undertaking some form of optical signal processing prior to transduction back to the electrical domain.

As a preliminary task to achieve this aim, in this section a simple fibre-optic RF correlator which can be used for either instantaneous frequency measurement (IFM) or angle of arrival (AOA) determination (Ref 33) is proposed, and the results of measurements taken from a simple fibre-optic correlator are discussed.

The design concept is one of an all optical accessory to an optical RF link that can be used to enhance probability of intercept and signal sorting capability. The frequency resolution would be comparable to a conventional IFM, the complexity and maintenance minimal. The substantial advantages of the device would be

(a) extremely wide bandwidth (up to 40 GHz)

(b) moderate cost

(c) potential for having no active electronics at the antenna.

4.2 Theory of Operation

Figure 4.1 shows the basic component of the optical IFM - a simple fibre Mach-Zehnder interferometer. The delay τ plays the same role as in conventional IFM receivers (ie determines frequency response and ultimate resolution), with the added constraint that τ must be much greater than the coherence length of the optical source. This implies that the optical carriers are uncorrelated when mixed on the high speed photodiode.

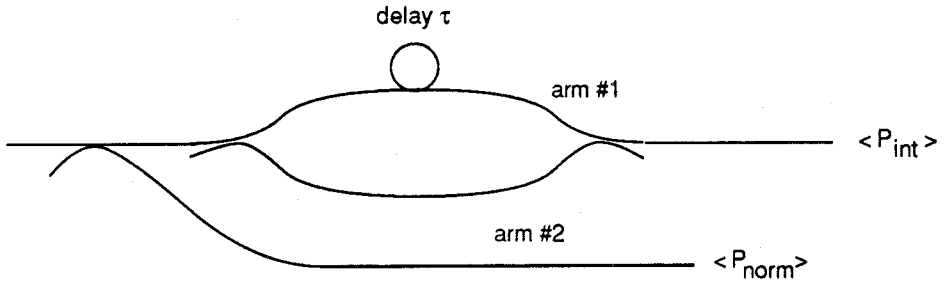

Figure 4.1 Fibre optic interferometer.

The power in each arm of the interferometer can be expressed in the general form

$$P = P_o \, Re \{ \exp (2\pi jft) \} + \overline{P} \qquad (4.1)$$

where

P_o - modulation depth (which is related to the RF input power)

f - RF modulation frequency

$\overline{P}$ average optical power in each arm (dc bias).

The power at the photodiode at time t is just (assuming perfect 3 dB splitters and combiners)

$$P_{pd} = \frac{1}{2} P_o \, Re \{\exp(2\pi jf[t-t_o]) + \exp(2\pi jf[t-t_o-\tau])\} + \overline{P} \tag{4.2}$$

where

t = 0 is taken at the input to the interferometer

t_o = time taken to traverse arm #2

τ = relative delay between arm #1 and arm #2

and the factor of $\frac{1}{2}$ accounts for 3 dB loss at the output coupler. Equation (4.2) can be re-expressed as

$$P_{pd}(t) = \{P_o \cos(\pi f\tau)\} \cos(2\pi f[t - to - \tau/2]) + \overline{P} \tag{4.3}$$

It is apparent from Equation 4.3 that the envelope of the output of the interferometer now contains frequency information, which is to be determined. The other unknown quantities are the modulation depth P_o (since the input RF power is unknown), and $\overline{P}$, the dc bias term, which will gradually vary with aging etc. The bias term actually presents no problem as it is easily eliminated by a dc block on the photodiode output. The unknown modulation amplitude can be removed by suitable normalisation by the original signal detected via a 3 dB coupler inserted prior to the interferometer. This signal will simply be of the form

$$P_{pd}(t) = P_o \cos(\pi ft) + \overline{P} \tag{4.4}$$

A simple power envelope detection circuit at the output of the normalising photodiode and the interferometer photodiode will then yield electrical output powers given by

$$\langle P_{norm} \rangle = \frac{k^2 P_o^2}{2} \tag{4.5}$$

$$\langle P_{int} \rangle = \frac{k^2 P_o^2 \cos^2(\pi f\tau)}{2} \tag{4.6}$$

ie

$$\frac{\langle P_{int} \rangle}{\langle P_{norm} \rangle} = \cos^2(\pi f\tau) \tag{4.7}$$

independent of RF input power and system frequency response (since the normalisation and interferometer diodes etc are identical). In passing it is interesting to note that cascading n identical interferometers yields an output of

$$\frac{\langle P_{int}^{(n)} \rangle}{\langle P_{norm} \rangle} = \cos^{2n}(\pi f\tau) \tag{4.8}$$

ie a periodic function highly peaked about the frequencies $f = \frac{m}{\tau}$, m = 0,1,2,...

This may be a useful feature for optical RF bandpass filtering applications.

4.3 Some Preliminary Numbers

It would be useful to have an IFM capable of at least covering the current EW bands of interest, so an initial maximum frequency of 20 GHz is chosen. The zero of the envelope function occurs at

$$f_m = \frac{1}{2\tau} \tag{4.9}$$

which implies a minimum delay of

$$\tau = 25 \text{ psec} \tag{4.10}$$

At the optical communications wavelengths of 1.3 μm and 1.5 μm, the refractive index of standard fibre is about 1.45 (Ref 34), and so Equation 4.10 implies a differential length between the interferometer arms of

$$\mathcal{L} = \frac{c\tau}{n} \approx 5 \text{ mm} \tag{4.11}$$

It is required that this differential length be much greater than the coherence length of the laser diode source. A typical multi-mode Fabry-Perot laser diode has a spectral width of the order of 3 nm (Ref 6). The coherence length is given by (Ref 35)

$$L_c = \frac{c}{2\pi\Delta\nu}$$

ie

$$L_c = \frac{\lambda^2}{2\pi\Delta\lambda} \tag{4.12}$$

which for λ = 1300 nm and $\Delta\lambda$ = 3 nm gives

$$L_c \approx 0.1 \text{ mm} \tag{4.13}$$

Thus $\mathcal{L} >> L_c$, and the analysis given in Section 4.2 should be valid.

Another aspect of interest to conventional IFM design is the thermal stability of the delay lines. Conventional IFM design requires either active thermal stabilisation of the longer delays or use of digital compensation techniques (Ref 36).

The time taken for light to travel a length L of fibre is just

$$t = \frac{nL}{c} \tag{4.14}$$

where n is the fibre refractive index and c is the speed of light. A change in temperature will result in a change in propagation time given by

$$\Delta t \approx \frac{1}{c}\left(n\frac{\partial L}{\partial T} + L\frac{\partial n}{\partial T}\right)\Delta T \tag{4.15}$$

Thus, the change in the differential delay τ can be written as

$$\Delta\tau \approx \frac{\mathcal{L}}{c}\left(n\left(\frac{1}{\mathcal{L}}\frac{\partial \mathcal{L}}{\partial T}\right) + \frac{\partial n}{\partial T}\right)\Delta T$$

ie

$$\frac{\Delta\tau}{\tau} = \left(\frac{1}{\mathcal{L}}\frac{\partial \mathcal{L}}{\partial T} + \frac{1}{n}\frac{\partial n}{\partial T}\right)\Delta T \qquad (4.16)$$

Typical values for the thermal expansion coefficient and refractive index temperature coefficient are (Ref 34,37)

$$\frac{1}{\mathcal{L}}\frac{\partial \mathcal{L}}{\partial T} \approx 3.4 - 5.5 \times 10^{-7} / {}^{\circ}C \quad \text{(bare fibre)}$$

$$\frac{\partial n}{\partial T} \approx 1.28 \times 10^{-5} / {}^{\circ}C \quad (0 \text{ to } 700^{\circ}).$$

Thus, the fractional change in the differential delay due to a temperature variation ΔT is dominated by the change in refractive index with temperature rather than thermal expansion, and is approximately

$$\frac{\Delta\tau}{\tau} \approx 10^{-5}\,\Delta T \qquad (4.17)$$

or, since

$$\frac{\Delta\tau}{\tau} = \frac{\Delta f_m}{f_m}$$

then

$$\frac{\Delta f_m}{f_m} \approx 10^{-5}\,\Delta T \qquad (4.18)$$

As long as the temperature variation ΔT is such that $10^{-5}\Delta T f_m$ results in a frequency inaccuracy less than that arising due to noise contributions, the fibre interferometer will not require any form of active stabilisation or compensation. This point shall be discussed in further detail in Section 4.5.

4.4 Testing the Frequency Response of a Fibre-Optic Microwave Interferometer

In order to test the theory of Section 4.2, and to check for effects due to laser frequency chirp or phase-induced intensity noise (the interferometer configuration will convert phase noise - unimportant in a direct detection link - into intensity noise which is then detectable), a simple cascaded-interferometer using multi-mode fibre was constructed. A schematic is shown in Figure 4.2.

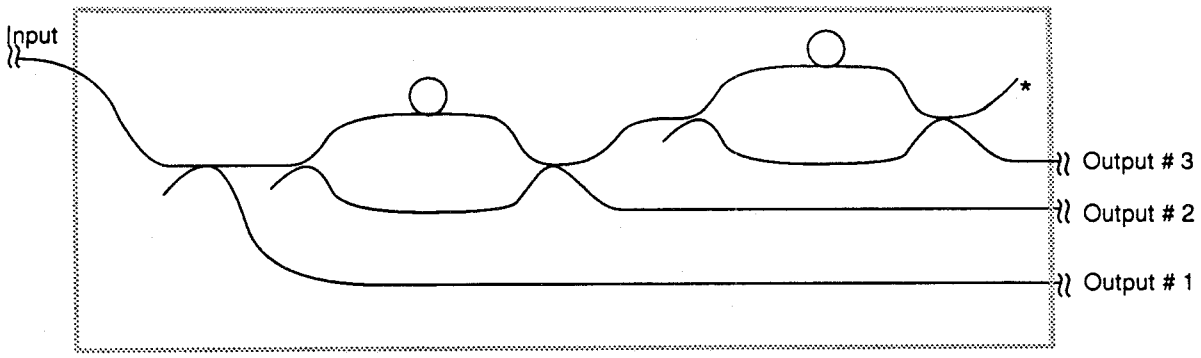

Figure 4.2 Cascaded fibre interferometer for microwave frequency measurement.

The optical source was a Lasertron QLM1300MW-002 10 GHz bandwidth directly modulated laser, and the detector was a matching QDEMW-002 10 GHz bandwidth detector. The fibre interferometer module measured 145 mm x 95 mm x 20 mm and weighed about 110 gms. Standard FC/PC fibre optic connectors were used to connect the laser and photodiode to the module. Output #1 was the straight-through link used to normalise the interferometer response. Outputs #2 and #3 should exhibit frequency responses proportional to $\cos^2(\pi f\tau)$ and $\cos^4(\pi f\tau)$ respectively. The microwave source was a Wiltron 6769A and the output power at each frequency was measured using a Hewlett-Packard HP8562A spectrum analyzer.

Initially, the insertion loss of the link was checked at an input frequency of 2 GHz. It was found that the insertion loss was surprisingly large, being, for each arm

$\rho_L(\#1) = 60$ dB

$\rho_L(\#2) = 65$ dB

$\rho_L(\#3) = 70$ dB

The general magnitude of these measurements was re-confirmed at an input frequency of 500 MHz, where the effect of the interferometer responses would not be very significant. It was also found that the output was sensitive to torsional stress on the input fibres, with maximum variations of up to 10 dB. The Q-LINK-10 system has a quoted insertion loss of < 35 dB, and so of the order of 30 dB was unaccounted for. It is thought the excess loss is due to the fact that multi-mode fibre is used for the interferometer, but the light is launched from a single mode fibre. This means that the modal distribution of light within the multi-mode fibre would initially be unknown, but would gradually evolve as the light propagated down the fibre (the mode distribution is said to be "underfilled"). Typically, the steady-state modal distribution would not be achieved until after several hundreds of metres, or even several kilometres, of propagation. Since the 3 dB couplers were constructed for multi-mode fibre with a steady-state modal distribution, it is probable that only certain modes from the diode laser are coupled out at each splitter. If most of the laser energy remains in the primary fibre at each coupler, then the particular configuration shown in Figure 4.2 would result in most of the power initially coupled into the fibre being lost to the unused output (marked by the * in Figure 4.2), and a high insertion loss would result. The response of the output to torsional stress on the input fibre would support this hypothesis, as stress would lead to a more rapid re-distribution of the launched modes.

Other possibilities of course include connector alignment losses or simply faulty transmitter or receiver modules. These could not be checked at the time due to lack of appropriate facilities. If the excess loss is due to a non-equilibrium modal distribution, addition of a mode scrambler on the input fibre should rectify this without causing undue losses.

The measurements were taken with the input and output fibres taped down to avoid accidental or varying stresses during data acquisition, and the low power levels meant that a detection bandwidth of 1 MHz had to be used - a figure that is about 2 orders of magnitude smaller than

would have been ideal (a 10 ns acquisition time is about normal for an IFM (Ref 36,38)). The RF input power was nominally +10 dBm. Due to a lack of equipment, measurements across the full frequency band were made at each fibre output sequentially, not simultaneously.

Figure 4.3 shows the average output power from the signal generator measured using an HP power head and suitably calibrated HP power meter.

Figure 4.4 shows the fibre-optic link frequency response normalised against the RF input power. The characteristic resonance peak around 10 GHz and 40 dB/decade drop in response after the peak are apparent.

Figure 4.5 shows the single-interferometer response from output #2 normalised against the system response, output #1. Figure 4.6 is the equivalent linear plot, showing the characteristic $\cos^2$ shape. The curve is a best least-squares fit, indicating a differential delay of

$$\tau = 0.1015 \pm 0.0014 \text{ nsec.}$$

The error bars on the second and tenth points indicate "recording error" ie the powers (in dBm) were only recorded to one decimal place, so the error bars reflect the ± 0.05 dBm recording accuracy.

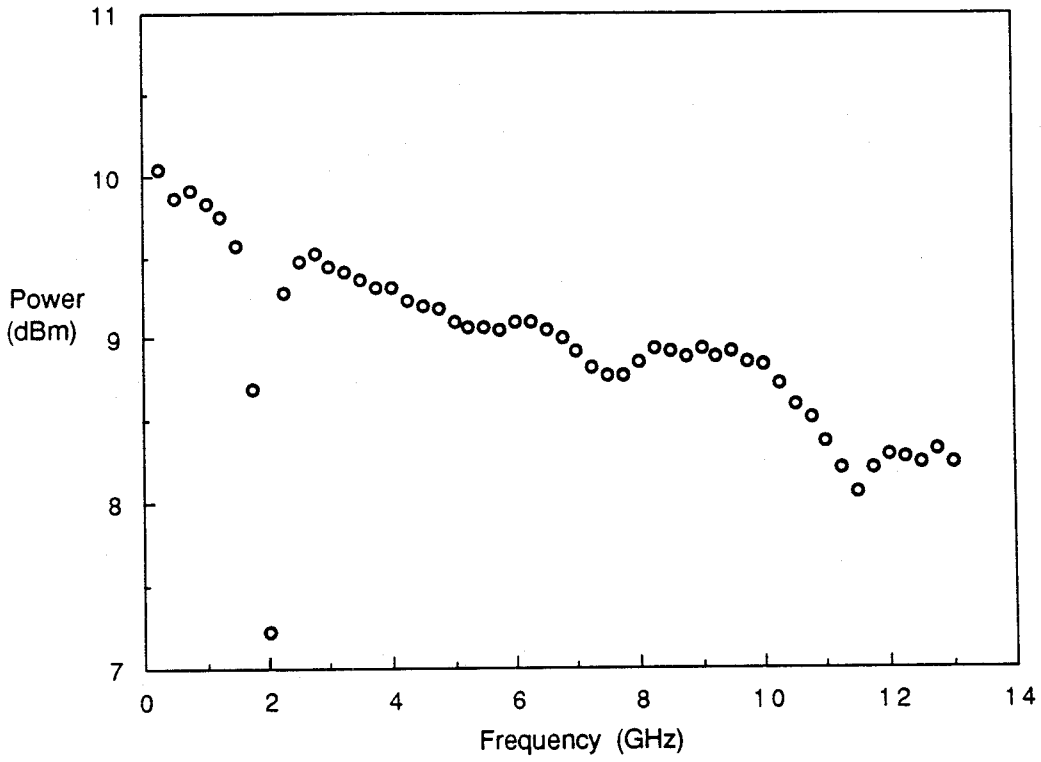

Figure 4.3 Output from signal generator.

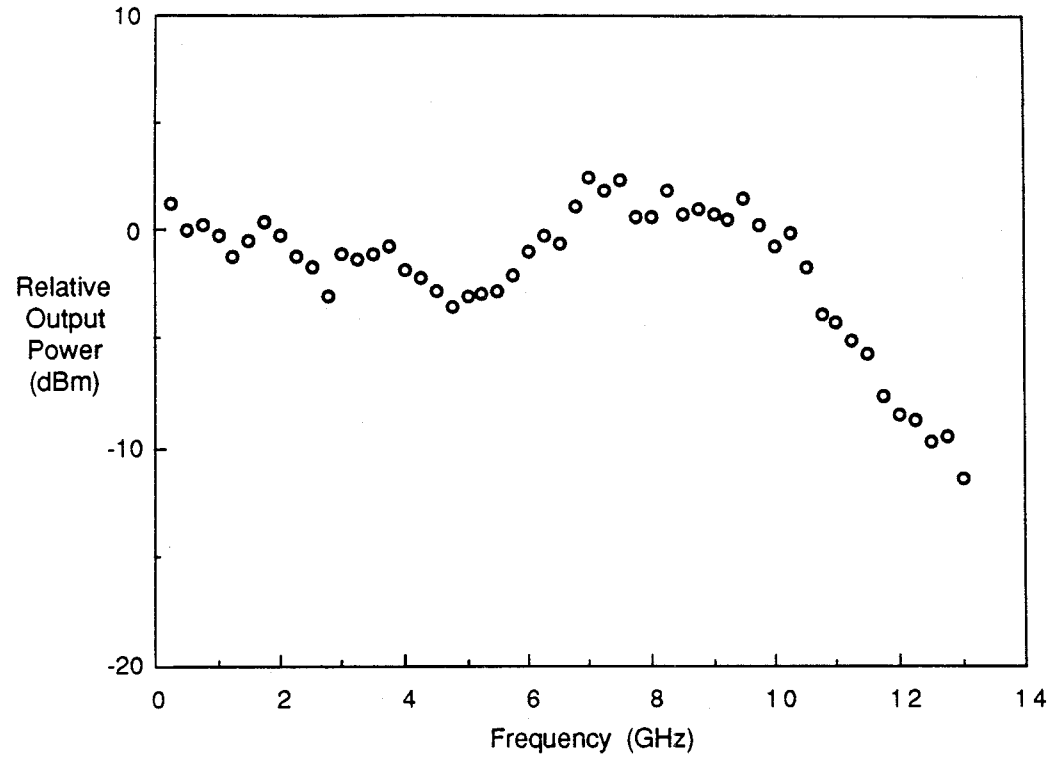

Figure 4.4 Normalised system frequency response from output #1.

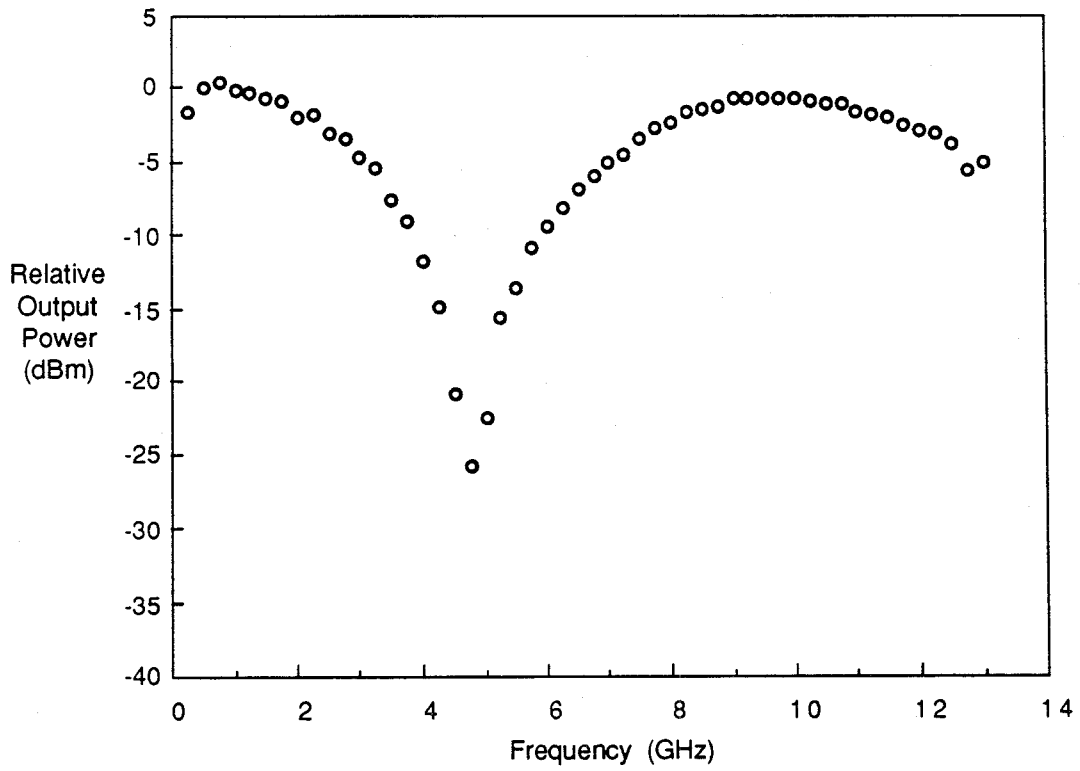

Figure 4.5 Fibre interferometer response.

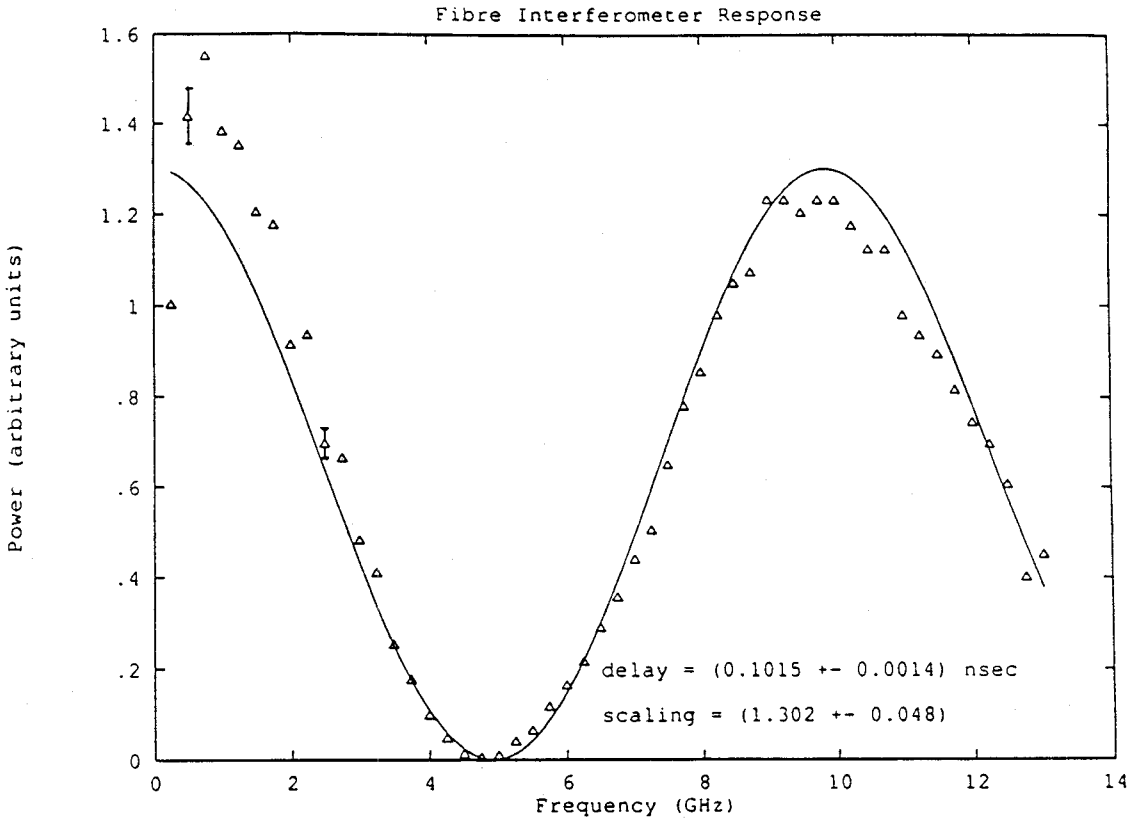

Figure 4.6 Fibre interferometer response.

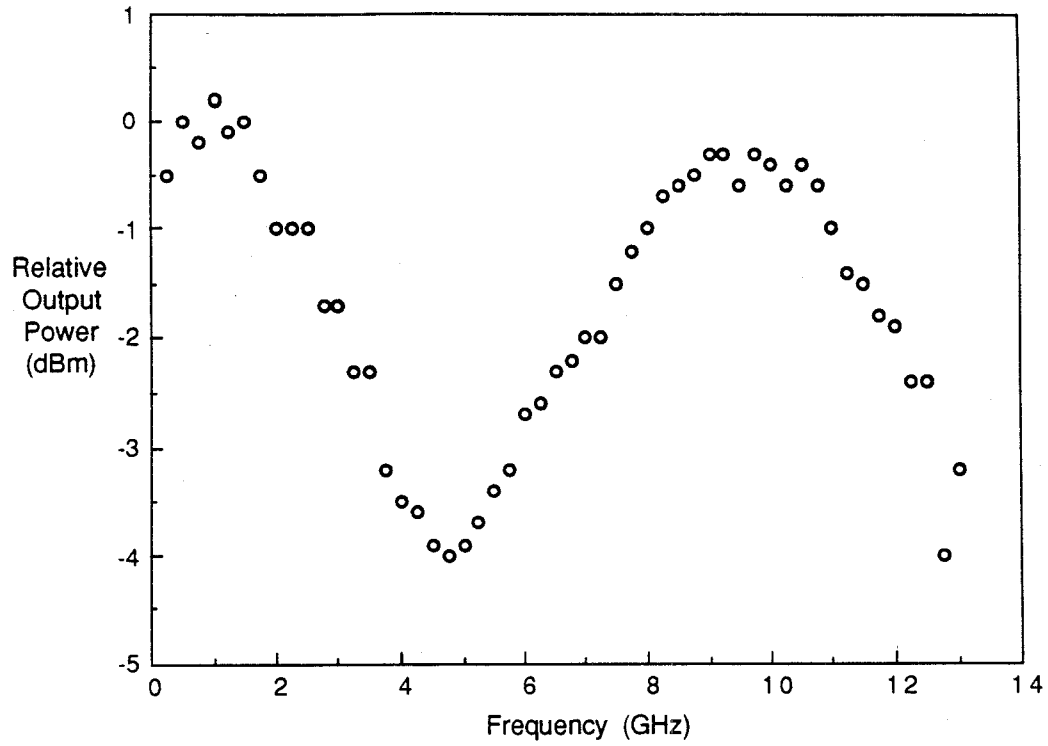

Figure 4.7 Response from output #3.

Figure 4.7 shows the two-stage interferometer response. Whilst there is clearly some frequency dependence, it is apparent that it is quite noisy and somewhat similar to the system frequency response. It is thought that this graph represents a sum of the system response, a $\cos^2$ response and some $\cos^4$ response, attributable to the vagaries of the coupling characteristics of the "underfilled" fibre (under such conditions it is basically luck that the single interferometer showed such a clear response).

Considering that

(1) throughput losses of ~ 60 dB were incurred,

(2) the measurements for each arm were taken about an hour apart (leading to interferometer response measurements being normalised against system response measurements taken one to one and one-half hours previously),

(3) the fibres themselves exhibited large stress sensitivity,

it is concluded that the results are quite promising.

It will be necessary to repeat this experiment with the following modifications -

(1) optical isolator on the input fibre,

(2) either:

  (a) mode scrambler on input if multi-mode fibre is used, or

  (b) use single mode fibre,

(3) purchase enough high-speed diodes to allow simultaneous measurements of all interferometer outputs,

(4) purchase basic fibre-optic accessories (eg a simple single mode fibre cable, the optical equivalent of a length of co-axial cable, would have been extremely useful).

The original cost of construction of the cascaded interferometers was only $2K. The suggested modifications would mean the expenditure of approximately a further $15K to properly investigate the viability of the device.

4.5 Optical IFM - General System Considerations

In this section general system considerations such as how an optical IFM system might be configured, the advantages of such architectures and theoretically attainable frequency resolution are discussed.

Figure 4.8 shows a possible architecture for an optical IFM. The RF input is fed directly to an electro-optic modulator, the optical signal is amplified using a fibre-laser amplifier (Ref 39), and a 1 x 8 coupler distributes the power evenly to a normalisation arm, 6 interferometers (each with a different delay τ) and a straight through link to allow further signal processing if required. One immediate and obvious advantage of this configuration is that there are no active electronic components in the antenna head itself. This may be a highly desirable feature in many operational scenarios. Clearly, if necessary, the antenna can be a considerable distance from the processing interferometers. The optical amplifier will act as a very broad band microwave amplifier, and can be chosen so that the link insertion loss is minimised (there will, however, be the usual trade-off with shot noise at the detectors). The minimum gain of the optical amplifier stage would only need to be ~ 12 dB to compensate for splitting losses - an easily achievable figure (15 dB is obtainable from a commercially available device (Ref 39)).

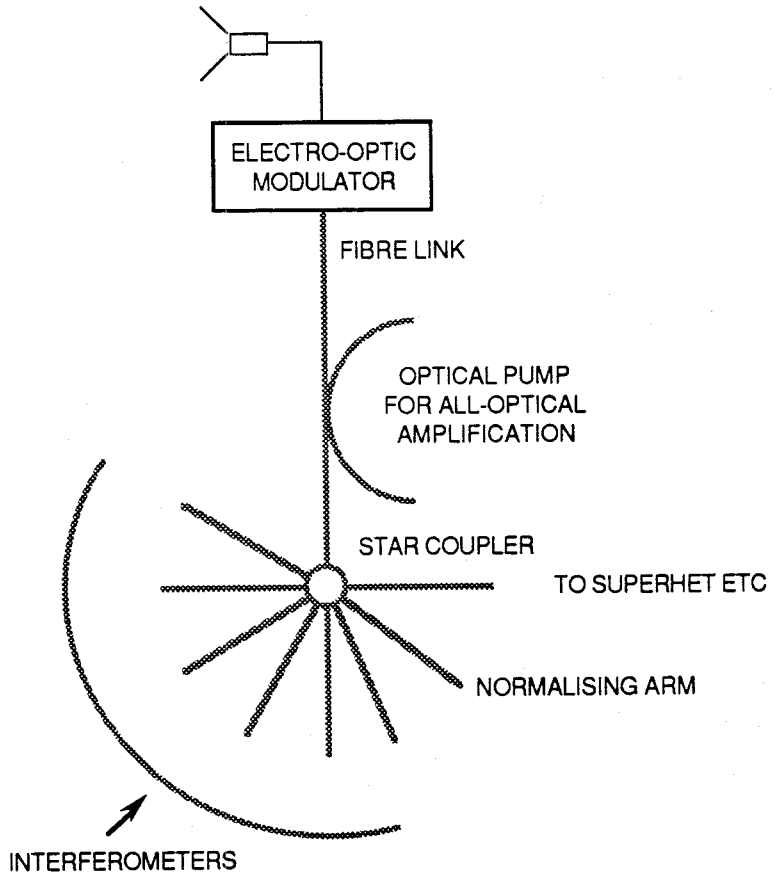

Figure 4.8 Optical IFM architecture.

Each of the interferometer arms can be treated as a separate microwave fibre-optic link, as was done in Section 2 (an extra 3 dB of noise can be added to the usual link calculation to roughly simulate the worst-case scenario of addition of correlated noise sources at the photodiode).

It is of interest to calculate the effect of the noise associated with the output of each interferometer in order to determine the fundamental frequency accuracy as a function of input power for a given delay τ. The electrical power output from the n^{th} interferometer is, from Equation 4.6,

$$\langle P_n \rangle = \frac{k^2 P_o^2}{2} \cos^2(\pi f \tau_n)$$
$$= \frac{k^2 P_o^2}{2} \cos^2\left(\frac{\pi f}{2 f_n}\right) \qquad (4.19)$$

As indicated in Figure 4.9, the maximum possible frequency ambiguity associated with a measurement uncertainty $< \delta P_n >$ occurs at the maxima and minima of the response. Therefore, a worst-case frequency error is obtained simply by expanding Equation 4.19 in a Maclaurin series and keeping the first terms, ie

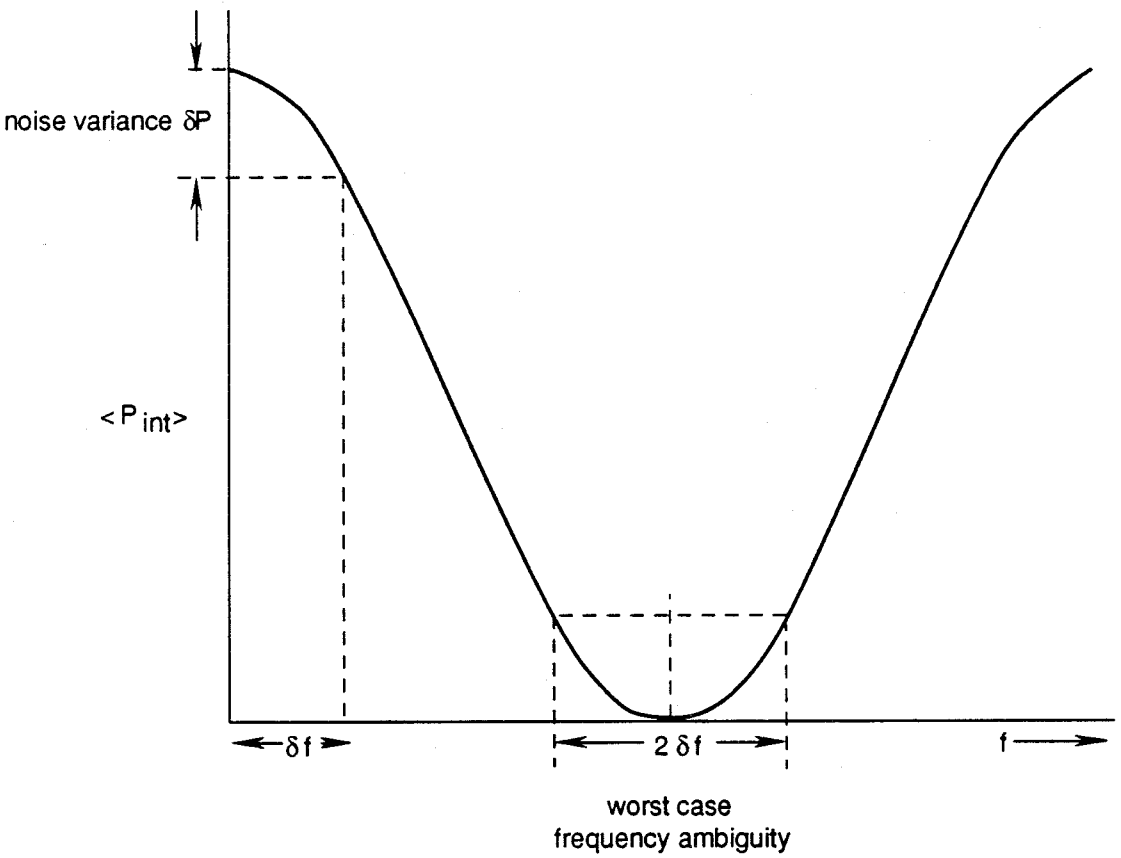

Figure 4.9 Uncertainty in frequency determination due to noise.

$$\langle P_n \rangle = \frac{k^2 P_o^2}{2} \cos^2\left(\frac{\pi f}{2f_n}\right)$$
$$= \frac{k^2 P_o^2}{4}\left(1 + \cos\left[\frac{\pi f}{f_n}\right]\right)$$
$$\approx \frac{k^2 P_o^2}{2}\left(1 - \left(\frac{\pi f}{2f_n}\right)^2 + \ldots\right) \qquad (4.20)$$

where P_o is the average power of the RF signal measured by the normalising detector. A measurement uncertainty $< \delta P_n >$ then corresponds to a frequency error of approximately

$$\langle P_n(0) \rangle - \langle \delta P_n \rangle \approx \frac{k^2 P_o^2}{2}\left(1 - \left[\frac{\pi\, \delta f_n}{2f_n}\right]^2\right)$$
$$\Rightarrow \frac{k^2 P_o^2}{2} - \langle \delta P_n \rangle = \frac{k^2 P_o^2}{2}\left(1 - \left[\frac{\pi\, \delta f_n}{2f_n}\right]^2\right)$$
$$\Rightarrow \delta f_n = \left(\frac{k^2 P_o^2}{2\langle \delta P_n \rangle}\right)^{\frac{1}{2}} \frac{2f_n}{\pi} \qquad (4.21)$$

The quantity in the brackets is just the usual electrical SNR of the straight through link, and so

$$\delta f_n = \frac{2f_n}{\pi \sqrt{SNR}} \qquad (4.22a)$$

As indicated in Figure 4.9, the maximum possible error is actually twice this amount due to the symmetry of the interferometer response, and so

$$\delta f_n \approx \frac{1.3\, f_n}{\sqrt{SNR}} \qquad (4.22b)$$

Each of the fibre differential delays should be tailored such that

$$f_1 = f_{max} \qquad (4.23)$$

$$f_n = \delta f_{n-1},\ n \geq 2. \qquad (4.24)$$

As an example, for a maximum bandwidth coverage of 20 GHz and SNR = 22 dB, have

f_n	δf_n	units
20	2	GHz
2	0.2	GHz
200	20	MHz
20	2	MHz

ie, only 4 interferometers are required to achieve 2 MHz resolution across the full 20 GHz, for a SNR ≥ 20 dB.

It should be emphasised that the example calculation does not account for the beneficial effect obtained from normalising the response of the interferometer against the reference arm. For example, for a differential delay τ and appropriate choice of propagation time of the reference

arm, noise with frequency components $f<<1/\tau$ will effectively be normalised out of the final ratioed signal. Similarly, noise with frequency components much greater than the inverse of the sampling time will be averaged in the sampling process, and as such will contribute less. Thus, for the highest frequency interferometer in the example given above, the noise components $f<<40$ GHz will be ratioed out of the response, whereas (assuming a 10 ns sampling time) the spectral components much greater than 100 MHz will be averaged in the sampling. The very large overlap of these two "averaging windows" implies that the resolution will be substantially improved for a given SNR than is implied by Equation 4.22b. It is clear that the resolution attainable will decrease as the differential delay τ increases. Hence, to keep with worst-case performance estimates, the resolution and required SNR's implied by Equation 4.22b will be used.

The thermal stability criterion, Equation 4.18 implies that

$$\frac{\delta f_n}{f_n} >> 10^{-5}\,\Delta T$$

$$\Rightarrow \Delta T << 10^4\ ^\circ C \qquad (4.25)$$

It is clear that for higher SNR's, the temperature variations will begin to limit the frequency resolution attainable by a single interferometer stage, however this will clearly be of limited significance for multiple interferometers.

At this point it is useful to calculate the details of a system based upon the capabilities of current technology. The system components, which are basically the system denoted E2 in Section 2 plus a fibre-optic amplifier and the IFM network, are listed below

Transmitter

- 40 GHz bandwidth modulator, $V_\pi = 7.5$ V, optical insertion loss = 3.5 dB (Ref 16)
  $R_{in} = 50\ \Omega$, $\sigma_{TX} = 1.0$ {L}
- no RF pre-amplification
- 30 mW optical power delivered into modulator via remote laser diode {C}

Link

- 1 km single mode fibre, attenuation - 0.3 dB/km {C}
- all-optical fibre amplifier to provide ~ 27 dB (optical) amplification prior to the 1 x 8 fibre couplers {L}
- 1 x 8 fibre coupler, distributing optical signal to {C}
  - (a) normalising arm,
  - (b) 6 x fibre interferometers,
  - (c) normal straight link to allow further signal processing if required.

- interferometer delays {C} : f_1 = 40 GHz
  f_2 = 10 GHz
  f_3 = 2.5 GHz
  f_4 = 630 MHz
  f_5 = 160 MHz
  f_6 = 40 MHz

  $\Rightarrow$ shortest differential delay = 12.5 ps $\approx$ 2.4 mm

  $\Rightarrow$ longest differential delay = 12.5 ns $\approx$ 2.4 m

Detection

- 60 GHz bandwidth photodiodes (Ref 40) {C} with assumed parameters

  r = 0.7 mA/mW

  R_L = 50 Ω

  σ_{RX} = 1.0.

- 40 GHz diode to enable square law detection {C}

- 10 ns settling time sample and hold {C}

The notations {C} and {L} denote "commercially available" and "laboratory demonstrator" respectively.

The fibre amplifier is assumed to be noiseless and is there to compensate for link losses not accounted for in the calculations done in Section 2, ie ~ 9 dB due to the 1 x 8 coupler and ~ 3 dB at each interferometer output (this last is somewhat unnecessary since there is no requirement that the outputs be recombined to be within the one fibre. If required the output from the two separate arms can be added directly on the photodiode without the need for the final coupler - there is clearly a substantial advantage in doing this). The final result is that the calculations carried out previously are valid for each interferometer arm, and so each interferometer has the characteristics

insertion loss ~ 26 dB

EIN ~ -137 dBm/Hz

where an extra 3 dB in noise has been added to account for correlated noise at the photodiode (a worst case approximation). The 10 ns setting time for the sample and hold implies a detection bandwidth of ~ 100 MHz (ignoring aliasing), and so the noise power referred to the input of the modulator is

$$\langle \delta P(\text{input}) \rangle = -57 \text{ dBm} . \tag{4.27}$$

Using the results of Section 2 for a perfectly biased modulator and 100 MHz detection bandwidth, the maximum input power at the modulator is found to be

$$\langle P(\max) \rangle = -2.0 \text{ dBm} \tag{4.28}$$

giving a spur free dynamic range of

$$SFDR = 55 \text{ dB} . \tag{4.29}$$

The interferometer delays (Equations 2.47) have been conservatively chosen such that $\frac{\delta f_n}{f_n} \approx 0.25$ which from Equation 4.22 implies a minimum required signal to noise ratio of 14 dB, and a maximum frequency resolution of 4 MHz. Thus the actual system sensitivity and operational dynamic range are

$$S = -43 \text{ dBm} \tag{4.30}$$

$$DR = 41 \text{ dB} \tag{4.31}$$

Figure 4.10 shows the theoretically attainable frequency resolution as a function of SNR. Several advantages occur for SNR's greater than 14 dB. These include both a higher resolution (as given by Equation 4.22) and, for sufficiently high SNR's, the necessity of interrogating fewer than 6 interferometers. For example, for an input power of -23 dBm (34 dB SNR), only interferometers 1, 3 and 5 need be interrogated to achieve an ultimate resolution of 4 MHz. Another advantage in high SNR's is that the minimum analysable pulse width (given essentially by the delay associated with the longest delay line plus the sample and hold settling time) decreases, since the longest delay which needs to be used to obtain satisfactory frequency resolution decreases.

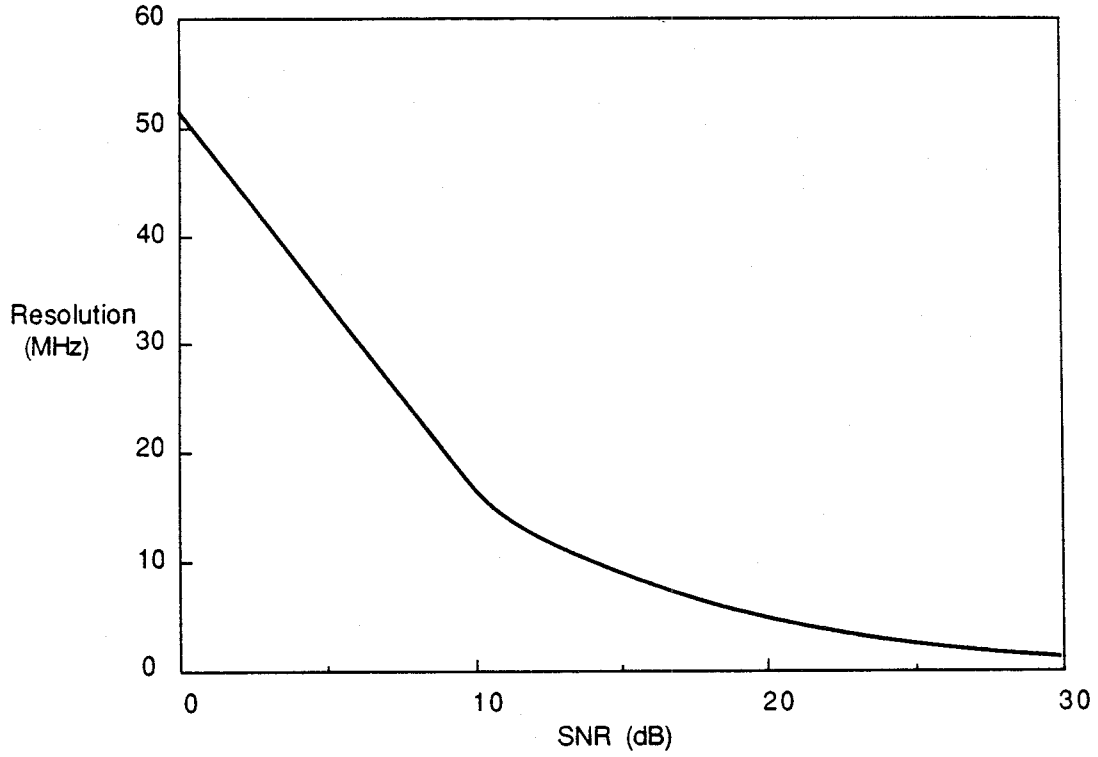

Figure 4.10 Frequency resolution of fibre IFM as a function of SNR.

Thus, the system performance specifications for worst case operation are

Frequency range:	1 to 40 GHz
Frequency resolution:	≤ 10 MHz
Minimum pulse width:	23 ns
Dynamic range:	-43 to -2 dBm

The Northern Scientific Laboratory NSL-1081 IFM subsystem (Ref 38), for comparison purposes, has the specifications

Frequency range:	7.5 to 18 GHz
Frequency resolution:	3 MHz
Minimum pulse width:	15 ns
Dynamic range:	-65 to -5 dBm

There are several important points to note when comparing these specifications:

1. Resolution of the optical IFM is theoretical resolution based on contributing noise sources - actual resolution would depend on how the detection system was physically implemented. Also, fibre amplifier noise was neglected (a typical noise figure for a fibre amplifier is ~ 7 dB (Ref 39), so the approximation should be quite good).

2. The optical IFM architecture described assumes no pre-amplification stages (to avoid having active electronics in the antenna), whereas the figures for the NSL-1081 include automatic gain control and limiting amplification at the input.

3. The sensitivity quoted for the optical IFM is referred to the power at the modulator (nominally 1 km from the interferometers), whereas the sensitivity for the NSL-1081 is referred to the input of the IFM module. This clearly indicates the potential usefulness of optical fibre-amplification techniques.

4. As discussed previously, no reduction in noise contributions due to normalisation against the reference arm or averaging on the sample and hold have been taken into account.

Considering these points, the theoretical performance of the optical IFM is very competitive. If necessary, the system sensitivity can be improved by the inclusion of appropriate broad-band pre-amplifiers prior to the electro-optic modulator. An example of an appropriate amplifier would be that developed by Yuen et al (Ref 29), which has the characteristics

Frequency range:	5 - 40 GHz
Gain:	12.5 dB
Noise figure:	< 4 dB.

Using this single pre-amplifier, the system sensitivity would be improved to ~ -56 dBm. Recent research into optical delivery of electrical power (Ref 41) indicates the possibility of maintaining total electrical isolation of the antenna despite having some active elements requiring biasing, power supply etc. It is now possible to deliver the required power optically, thereby avoiding the need for batteries (the optical component can provide 6 - 12 V dc), while retaining the obvious advantages of security and reduced susceptibility to electromagnetic interference (EMI) associated with fibre-optics.

It should be emphasised that the possibility of implementing such a broad-band IFM so easily arises solely due to the broad-band nature of fibre-optics. The couplers are 3 dB over very wide (RF) bandwidths, there is negligible dispersion, very small attenuation and minimal temperature dependence.

One consequence of the negligible dispersion and attenuation properties is that the periodic interferometer responses can extend out well past the 100 GHz region. In situations where there is a large discrepancy in signal densities (as is the case between the 0 - 20 GHz and 20 - 40 GHz regions), the addition of some simple pre-filtering and broad-band switching would allow the possibility of designing the interferometer delays for the 20 GHz band (thereby increasing the

resolution by a factor of 2), but when activity is detected in the 20 - 40 GHz band (by a simple crystal video detector), the 20 - 40 GHz band could be switched through the interferometers. The lack of dispersion and attenuation means that the interferometer outputs will still be able to be used to uniquely determine the frequency. This is shown schematically in Figure 4.11.

In summary, in this section an all-optical IFM receiver has been proposed. The performance of the receiver is comparable to that of conventional IFM's, however the optical version has the advantage of greater bandwidth, no thermal compensation is required, total electrical isolation of the antenna can be achieved and greater flexibility in signal processing is attainable. By using the spare output to correlate against the signal received from other antennas, angle of arrival information can also be determined (in this case the signal delays are due to different propagation times to each antenna rather than fibre-optic delays). Alternatively, if SNR ratio is very poor, the spare output can be delayed and sent to a scanning super-heterodyne receiver, which has been set to scan the reduced frequency band that the IFM *was* able to determine.

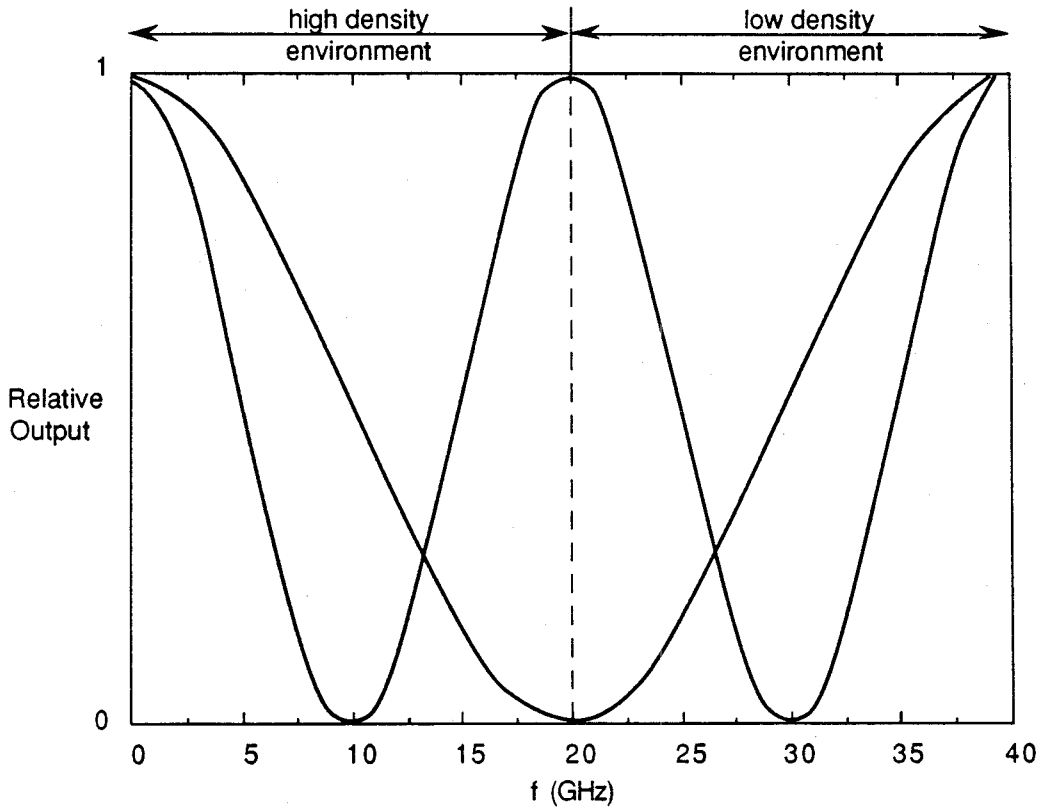

Figure 4.11 Schematic showing how a single set of interferometers can be used for different frequency regions.

4.6 The Role of Bulk Optics

While it is probably preferable to exploit guided-wave architectures in many operational environments, there are a number of practical advantages to investigating the potential role of bulk optical components to build devices such as the optical IFM. An optical IFM such as that described can be constructed very simply from a beam splitting cube and a mirror, as shown in Figure 4.12. The beamsplitting cube (which is commercially available with edge lengths as small as 5 mm), is simply given a reflective coating on one surface and an anti-reflective coating on the surface facing the mirror, resulting in a classical Michelson interferometer configuration. The advantages of this architecture are

(1) the device can be manufactured, coated and aligned on-site at DSTO

(2) the frequency response is tunable by adjusting the mirror distance

The fact that the device can be fabricated on-site is clearly advantageous in terms of program support.

A tunable frequency response may be useful in environments where the presence of a friendly emitter may be tuned out by selecting the "notch" in the frequency response to correspond to the transmission frequency of the friendly emitter, or where the interferometer response is to be optimised under varying signal environments to enhance detection probability of a particular emitter. A prototype bulk optics version of the cascaded interferometer described in Section 4.4 has been constructedat DSTO Salisbury, but testing of this device has not proceeded to date due to lack of appropriate equipment. Figure 4.13 is a schematic of the device, showing the expected outputs.

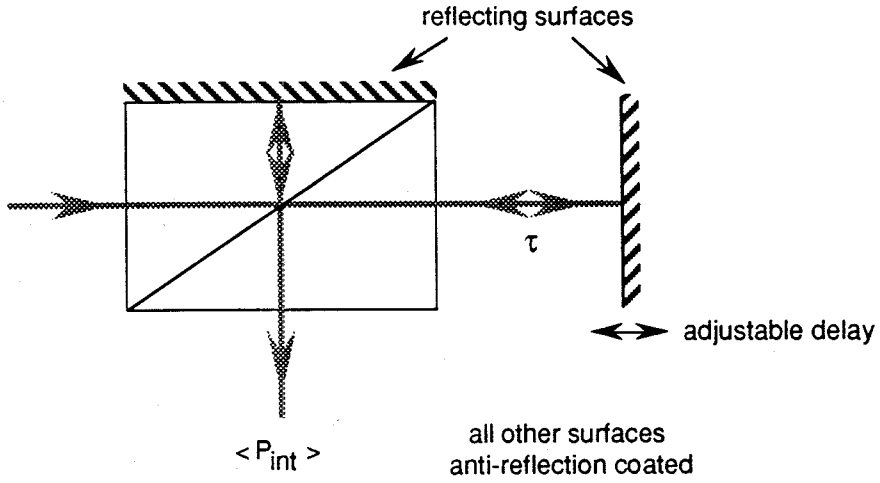

Figure 4.12 A tunable bulk optic interferometer.

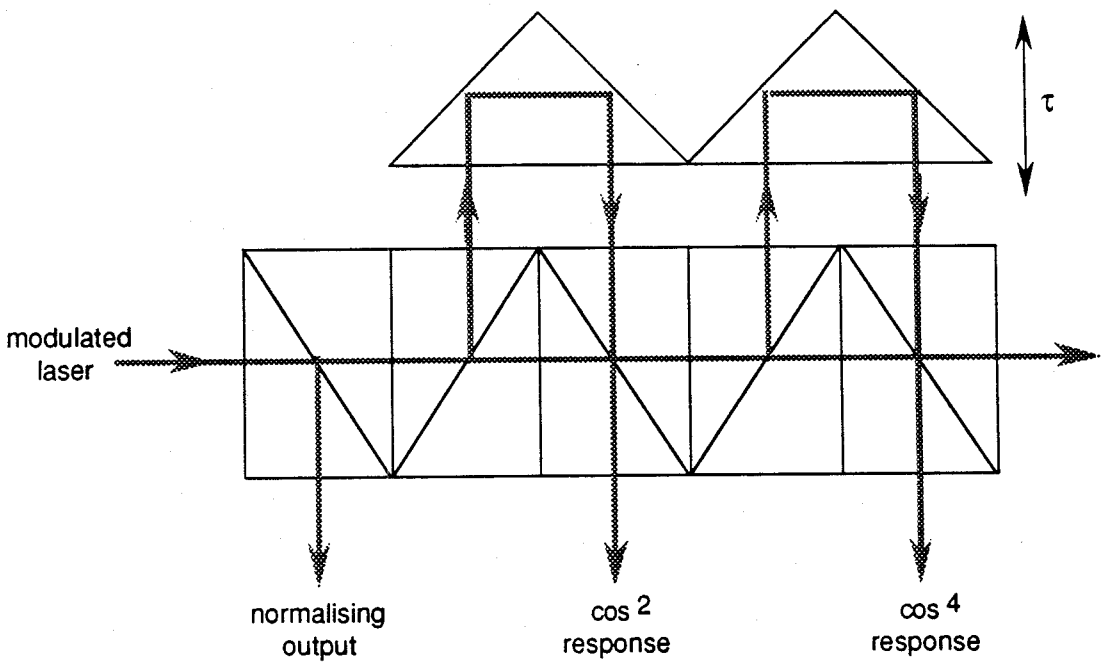

Figure 4.13 Cascaded microwave Mach-Zehnder interferometers.

5 CONCLUSIONS

5.1 Introduction

In this final section the results of this work are summarised and suggestions pertaining to appropriate directions for photonics research in Electronic Warfare Technology Group are discussed. In Section 5.2 the general research directions and the motivations for those directions are summarised. In Section 5.3 possible worthwhile projects mentioned in the text are again highlighted.

5.2 Wideband Photonics Research in Electronic Warfare Division

As discussed in Section 2.4, appropriate research activities must lead to significant improvements in the operational performance of photonics-based microwave/millimetre wave electronic warfare systems. As was also noted, this can only legitimately be addressed by first defining an operational scenario, which then establishes the system parameters of importance. The generic requirements of electronic warfare are, in order of importance:

(1) maximum bandwidth

(2) maximum sensitivity

(3) maximum dynamic range

In fulfilling these generic requirements, it is clear from both theoretical and demonstrated device performance considerations that wideband external electro-optic modulators offer superior performance when compared to direct modulation devices. It must be stressed however that for a *specific* scenario (as illustrated by the example of the towed aerial decoy of Section 3.3), a direct modulation solution may be preferable.

A further reason for establishing a strong research effort in integrated optical technology is the fact that Australia has *all* the required technological capability and expertise to undertake world class research into these devices. As previously noted, the basic inexperience of Australian researchers in the general development of very wide bandwidth millimetre wave devices using MBE techniques means that it would be extremely difficult to achieve significant breakthroughs in high speed laser diode research.

Finally, there are good commercial reasons for establishing a strong integrated optics capability - as shown in Table 1, which is an extract from the 1989 "Critical Technologies Plan" for the Committees on Armed Services of the United States Congress (Ref 42). While recognising that the major NATO countries and Japan will have substantial research efforts in all fields of interest, it is encouraging to note the possible niche for Australia that is indicated in the table in the area of integrated optics research (Item 7).

Thus, it is the conclusion of the author that a substantial research effort directed toward the development of wideband integrated optic modulators, the linearisation of the response of these devices, and the reduction of the insertion loss (preferably via the improvement of optical parameters such as low V_π structures and reduced optical loss), will be of long term benefit for EW applications. A preliminary concept demonstrator project is already underway to develop a modulator with a bandwidth of 5-6 GHz. An appropriate second phase of this program would be to extend this performance to cover the full 20 GHz EW microwave band of interest, and the third phase would attempt to push this limit to at least 40 GHz. It is the opinion of the author that if it is decided to pursue integrated optics research in any serious manner, substantial funding will have to be committed in order to establish a worthwhile program that is capable of producing quality results in a reasonable time frame.

Table 1 Countries with Significant National R&D Efforts
(other than the US, Japan, USSR; or NATO, or Warsaw-Pact Bloc).
(from (Ref (42))

Critical Technologies	Country
1. Microelectronics Circuits and Their Fabrication	India, S. Korea, Taiwan
2. Preparation of GaAs and Other Compound Semi-Conductors	China (for microwave applications)
3. Software Producibility	Brazil, India, Israel, Sweden
4. Parallel Computer Architectures	
5. Machine Intelligence/Robotics	Switzerland
6. Simulation and Modelling	
7. **INTEGRATED OPTICS**	
8. Fibre Optics	Brazil, China, Indonesia, S. Korea, Taiwan
9. Sensitive radars	China, Israel
10. Passive Sensors	Israel
11. Automatic target Recognition	Israel
12. Phased Arrays	Israel
13. Data Fusion	
14. Signature Control	China, Israel, Sweden, Switzerland, Taiwan
15. Computational Fluid Dynamics	China, Taiwan
16. Air Breathing Propulsion	China, India, Israel, Sweden, Taiwan
17. High Power Microwaves	China
18. Pulsed Power	China, Israel
19. Hypervelocity Projectiles	China, Israel, Sweden
20. High-Temperature/High-Strength/Light-Weight Composite Materials	Australia, Brazil, China, India, Israel, Sweden, S. Korea, Switzerland, Taiwan
21. Superconductivity	China, Switzerland
22. Biotechnology Materials and Processing	Many Countries

* *Since there are significant efforts related to each of the critical technologies in all the countries (or national groups) listed (under the title), these countries are not repeated in the table.*

5.3 Possible Research Projects

The opportunities offered by exploiting the unique advantages of optical techniques should not be minimised by attempting to directly apply conventional microwave doctrine or by taking too narrow a perspective on the possible benefits that accrue from the use of this rapidly maturing technology. As a classic example, fibre optic technology is obviously extremely well suited for use in the construction of microwave and millimetre wave delay lines, which are highly useful devices in electronic warfare. To embark on a research program with the *sole* aim of building longer or wider bandwidth delays however is not, in itself, either inspiring research or establishing an environment conducive to the development of novel concepts. The major emphasis of research should be to develop a novel *system* that will result in an enhanced defence capability for the ADF. The fact that the system may contain as a *component* a delay line that may be impressive when compared to standard technology should correctly be seen as simply a contribution to the overall product.

In the various sections of this report have been suggestions or examples of components and systems that may offer novel and useful research products. These are:

(a) development of extremely wide bandwidth electro-optic modulators and switches for EW applications

This area is fundamental to the usefulness of optical techniques to the EW arena, and includes considerations such as reduction of insertion loss and linearisation of response, as discussed in Sections 2 and 3.5

(b) development and application of fibre all-optical amplifiers for wide bandwidth systems

A method of microwave signal amplification without leaving the optical domain will also be essential in systems that have large losses that arise through either optical attenuation (long links, lossy system components etc) or through parallel pathway systems (such as the optical IFM concept).

(c) development of an all optical adjunct for signal processing (IFM or AOA determination)

Such an adjunct to conventional signal processing systems could act as a coarse pre-sorter or used to enhance probability of intercept of signals ie in general improvement of the performance of conventional systems. Such a concept was discussed in Section 4.

(d) development of an all optical link for a submarine EW mast

The small size, wide bandwidth and minimal support electronics requirements of an electro-optic modulator make this an attractive project. An example was discussed in Section 3.2.

(e) development of an expendable, remotely deployable EW mast for submarines

This concept was again briefly discussed in Section 3.2.

(f) development of an all-optical link to a towed decoy

The advantages of such a link would be the possibility of maintaining excellent phase coherence of the re-radiated signal and the elimination of microwave leakage from the tow cable. This is an example where a very long, tapped delay could be used for signal storage rather than a digital RF memory, however the overall project emphasis should be directed towards the *system* concept rather than the delay line *component*. This system was examined in Section 3.3. To avoid constructing very long optical delays, it may be worthwhile pursuing an optical recycling delay that allows a digital RF memory (which in general have very limited sampling accuracy - typically one or two bits) to sample a signal a number of times, thereby improving the digitisation of the signal and its subsequent reproduction.

In conclusion, photonics technology has advanced to the stage where useful EW systems spanning the traditional 18 GHz EW regime can be constructed from off-the-shelf components. Useful devices spanning the regime up to 40 GHz have already been demonstrated. The unique properties of photonics systems and the possible niche in the world market for the products of Australian research must be exploited by innovative research programs that fully reflect the potential of this technology.

5.4 Addendum

For various reasons the better part of twelve months has elapsed between the first draft of this document and the final product. As an indication of the rapidity of evolution of the photonics field a number of significant developments are included in this addendum:

1. An 18 GHz bandwidth directly modulated laser diode has become available as a result of the USAF contract alluded to in section 2.2.1. Known as the Q-LINK-005 system, its parameters are (Ref 43):

Bandwidth	-	18 GHz
Insertion loss (electrical)	-	40 dB
TOI	-	> 30 dBm
EIN	-	(-115 dBm/Hz 1-10 GHz
		(-110 dBm/Hz 10-18 GHz
SFDR	-	98 dB.$Hz^{2/3}$
Fiber coupled optical power		- 5 mW.

2. United Technologies Photonics (Ref 44) have introduced a 2 - 18 GHz bandwidth external modulator capable of handling up to 200 mW of optical power. This increased optical power results in a very significant reduction of link insertion loss. The device parameters are (Ref 44):

Bandwidth	-	2 - 18 GHz
Insertion loss (optical)	-	4.5 dB
Half wave voltage (V_π)	-	12 V
Optical power handling	-	200 mW

These figures indicate a link electrical insertion loss of 16 dB, which is sigificantly better than the 35 dB typical of directly modulated links and the 51 dB insertion loss calculated for system E1 of Section 2.3.3. The example applications of Section 3, in particular the towed decoy example, would also significantly benefit from the use of this commercially available device. The increase in power handling capability has arisen due to use of the annealed proton exchange integrated optic waveguide fabrication technique, as opposed to the more common technique of titanium indiffusion. This increased power handling capability is a very significant development in terms of increased utility of photonics technologies. Proton exchange based waveguides are being investigated by Monash University (Ref 45).

3. As noted in several sections of the report, development of wide-band amplification techniques is very important to the successful implementation of many photonic electronic warfare systems. A recent significant development in this field is the demonstrated local capability of producing 22 GHz bandwidth HEMT amplifiers (Ref 46). Designed by Electronic Warfare Division of DSTO and fabricated by CSIRO Division of Radiophysics, typical of the amplifiers is an 3 or 4 stage distributed amplifier showing 8 dB gain with less than 2 dB (absolute) ripple across the 1-22 GHz regime. This was the first attempt at designing such devices undertaken by Electronic Warfare Division, and the result is very encouraging for future work in extending both the gain and bandwidth of these components.

4. Improved (and very simple) designs have been proposed (Ref 47,48) which reduce modulator non-linearity - the major factor limiting the attainment of very large dynamic range of these devices. Dynamic ranges of the order of 100 dB are claimed.

REFERENCES

[1] R. Simons, Optical Control of Microwave Devices, Artech House, Boston, 1990.

[2] K. Uomi, T. Mishima and N. Chinone, "Ultrahigh Relaxation Oscillation Frequency (up to 30 GHz) of Highly p-doped GaAs/GaAlAs Multiple Quantum Well Lasers", Appl. Phys. Lett 51(2), p 78 - 80, 1987.

[3] A. Yariv, Quantum Electronics, John Wiley and Sons, New York, 1989.

[4] I. Suemune, L.A. Coldren, M. Yamanishi and Y. Kan, "Extremely Wide Modulation Bandwidth in a Low Threshold Current Strained Quantum Well Laser", Appl. Phys. Lett 53(15), pp 1378 - 80, 1988.

[5] "Fiber Optic Source and Detector Components", Lasertron Specification Sheet, 1989.

[6] "High Speed Fiber-Pigtailed GaAlAs Laser Diodes and Transmitters", Ortel Corp. Specification Sheet; "High Speed Fiber-Pigtailed GaAs Photodiodes and Receivers", Ortel Corp. Specification Sheet.

[7] RF/Microwave Fiber Optic Link Design Guide, Ortel Corp., 1989.

[8] C.H. Cox III, L.M. Johnson and G.E. Betts, "A Theoretical and Experimental Comparison of Directly and Externally Modulated Fiber-Optic Links", IEEE MTT-S Digest, 689 - 92, 1989.

[9] These values represent typical losses from commercially available fibre. Best mass-production figures are <0.16 dB/km (see, for example, Ref (31)).

[10] "Optical Fibre Fusion Splicer Type-35", Sumitomo Electric Specification Sheet, 1989.

[11] "Amphenol Interfuse Single Mode Fiber Optic Coupler" Amphenol Specification Sheet, 1989.

[12] H.W. Yen, C.M. Gee and H. Blauvelt, "High Speed Optical Modulation Techniques", Opt. Tech. Mic. Appl. SPIE 545, pp 2 - 9, 1985.

[13] T.E. Jenkins, Optical Sensing Techniques and Signal Processing, Prentice-Hall International, New Jersey, 1987.

[14] C.M. Gee, G.D. Thurmond and H.W. Yen, "17 GHz Bandwidth Electro-Optic Modulator", Appl. Phys. Lett 43(11), pp 998 - 1000, 1983.

[15] S.K. Korotky, G. Eisenstein, R.S. Tucker, J.J. Veselka and G. Raybon, "Optical Intensity Modulation to 40 GHz Using a Waveguide Electro-Optic Switch", Appl. Phys. Lett 50(23), pp 1631 - 3, 1987.

[16] D.W. Dolfi, M. Nazarathy and R.L. Jungerman, "40 GHz Electro-Optic Modulator with 7.5V Drive Voltage", Elect. Lett 24(9), pp 528 - 9, 1988.

[17] J. Nees, S. Williamson and G. Morou, "Greater than 100 GHz Traveling Wave Modulator", in Ultrafast Phenomena VI, Springer-Verlag, Berlin, 1988.

[18] "18 GHz Integrated Optical Amplitude Modulators", GEC Advanced Optical Products Specification Sheet, 1990.

[19] W.E. Stephens and T.R. Joseph, "System Characteristics of Direct Modulated and Externally Modulated RF Fiber-Optic Links", J. Light. Tech. LT-5(3), pp 380 - 7, 1987.

[20] M. Nazarathy, D.W. Dolfi and R.J. Jungerman, "Spread Spectrum Frequency Response of Coded Phase Reversal Traveling Wave Modulators", J. Light. Tech. LT-5(10), pp 1433 - 43, 1987.

[21] M. Nazarathy, D.W. Dolfi and R.J. Jungerman, "Velocity-Mismatch Compensation in Traveling-Wave Modulators using Pseudorandom Switched-Electrode Patterns", J. Opt. Soc. Am 4(6), pp 1071 - 9, 1987.

[22] A.R. Beaumont, C.G. Atkins and R.C. Booth, "Optically Induced Drift Effects in Lithium Niobate Electro-Optic Waveguide Devices Operating at a Wavelength of 1.51 mm", Elect. Lett 22(23), pp 1260 - 1, 1986.

[23] M. Digonnet, M. Fejer and R. Byer, " Characterization of Proton-Exchanged Waveguides in MgO:LiNbO3", Op. Lett 10(5), pp 235 - 7, 1985.

[24] G.E. Betts, L.M. Walpita, W.S.C. Chang and R.F. Mathis, "On the Linear Dynamic Range of Integrated Electrooptical Modulators", IEEE J. Quant Elec QE-22(7), pp 1009 - 11, 1986.

[25] BT&D Technologies PDC4304 In GaAs/InP High Speed Photodiode Specification Sheet, 1990.

[26] Watkins-Johnson Company, RF and Microwave Components Designer's Handbook, 1990-1991.

[27] Varian VTF-8290 A4 TWT Specification Sheet.

[28] T. Tamir (Ed.), Guided-Wave Optoelectronics, Springer-Verlag, Berlin, 1988.

[29] C. Yuen, Y.C. Pao, M. Day, C. Nishimoto, M. Glenn, S. Bandy and C. Zdasiuk, "Ultra-High Gain, Low Noise Monolithic hP HEMT Distributed Amplifier from 5 to 40 GHz", Elect. Lett. 26(8), pp 515-6, 1990.

[30] D. Wake, S.N. Judge, T.P. Spooner, M.J. Harlow, W.J. Duncan, I.D. Henning and M.J. O'Mahony, "Monolithic Integration of 1.5μm Optical Pre-Amplifier and PIN Photodetector with a Gain of 20 dB and a Bandwidth of 35 GHz", Elect. Lett. 26(15), pp 1166 - 8, 1990.

[31] S. Tanaka and H. Kanamori, "Singlemode Fibre for 1.55mm Long Distance Transmission System", Proc. 15th Aust. Conf. Opt. Fibre Tech., pp 97 - 100, 1990.

[32] R. Tucker, private communication.

[33] S.A. Pappert, M.N. McLandrich and C. Chang, "A Fiber-Optics Matched Delay Filter for RF Direction Finding", J.Light.Tech.LT-3(2), pp 273 - 6, 1985.

[34] Optics Guide 4 - Melles Griot Product Catalogue, 1988.

[35] W. Demtroder, Laser Spectroscopy, Springer-Verlag Berlin, 1982.

[36] J. Browne, "Discriminator Discerns Frequency From 6 to 10 GHz", Microwaves & RF, June, pp 220-2, 1988.

[37] H. Murata, Handbook of Optical Fibres and Cables, Macel Dekker Inc, New York, 1988.

[38] J. Browne, "IFM Subsystem Reads 15-ns pulses From 7.5 to 18 GHz", Microwaves & RF, December, pp 131-3, 1989.

[39] Fibre amplifiers BT&D/ EFA33000 Erbium Fibre Optical Amplifier, BT&D Preliminary Specification Sheet, 1990.

[40] Ultrahigh-Speed Photodetector, New Focus Inc. Specifcation Sheet, 1991.

[41] B.W. Henderson, "Varian Develops Technology to Send Power Via Fiber Optics", Aviation Week & Space Tech., August, pp 74-5, 1990.

[42] Critical Technologies Plan, prepared for the Committees on Armed Services of the United States Congress, March 1989.

[43] "QLINK-005 18 GHz Fiber-Optic Link", Lasertron Preliminary Product Summary,1992.

[44] "High Frequency Intensity Modulators", United Technologies Photonics Preliminary Data Sheet, 1992.

[45] L.N. Binh, private communication.

[46] G.A. Knight, private communication.

[47] P.L. Liu, B.J. Li and Y.S. Trisno, "In Search of a Linear Electrooptic Amplitude Modulator", IEEE Photonics Tech. Lett. 3(2), pp144 - 6, 1991.

[48] J.F. Lam and G.L. Tangonan, "A Novel Optical Modulator System with Enhanced Linearization Properties", IEEE Trans. Photonics Tech. Lett. 3(12), pp1102 - 4, 1991.

THIS IS A BLANK PAGE

DOCUMENT CONTROL DATA SHEET

Security classification of this page : UNCLASSIFIED

1 DOCUMENT NUMBERS		2 SECURITY CLASSIFICATION	
AR Number:	AR-006-950	a. Complete Document:	Unclassified
Series Number:	ERL-0617-RR	b. Title in Isolation	Unclassified
Other Numbers:		c. Summary in Isolation	Unclassified
		3 DOWNGRADING / DELIMITING INSTRUCTIONS	

4 TITLE

WIDEBAND GUIDED-WAVE PHOTONICS FOR ELECTRONIC WARFARE APPLICATIONS

5 PERSONAL AUTHOR (S)	6 DOCUMENT DATE
	March 1992
	7 7.1 TOTAL NUMBER OF PAGES
Anthony C Lindsay	72
	7.2 NUMBER OF REFERENCES
	48

8 8.1 CORPORATE AUTHOR (S)	9 REFERENCE NUMBERS	
Electronics Research Laboratory	a. Task:	DST 89/116
	b. Sponsoring Agency:	

8.2 DOCUMENT SERIES and NUMBER	10 COST CODE
Research Report 0617	798070

11 IMPRINT (Publishing organisation)	12 COMPUTER PROGRAM (S) (Title (s) and language (s))
Defence Science and Technology Organisation Salisbury	

13 RELEASE LIMITATIONS (of the document)

Approved for Public Release

Security classification of this page : UNCLASSIFIED

Security classification of this page : UNCLASSIFIED

14 ANNOUNCEMENT LIMITATIONS (of the information on these pages)

No limitation.

15 DESCRIPTORS		**16 COSATI CODES**
a. EJC Thesaurus Terms	Electronic warfare Photonics Modulation Microwaves Millimetre waves Bandwidth Integrated optics Fiber optics	200601
b. Non - Thesaurus Terms		

17 SUMMARY OR ABSTRACT
(if this is security classified, the announcement of this report will be similarly classified)

The report reviews the basic state of the art of guided-wave photonics systems for microwave and millimetre wave EW applications. Examples of several architectures are presented, and the results discussed in terms of Australian technological capability and current research in Electronic Warfare Division.